Diabetology & Metabolic Syndrome

RESEARCH

Open Access

Semaglutide and adenosine alleviate obesity-induced kidney injury, with observed modulation of the Txnip/NLRP3 pathway

Shuqi Wang[1,2], Xiaoyu Pan[4], Ruiqing Liang[1,2] and Shuchun Chen[1,2,3*]

Abstract

Objective This study was designed to evaluate the effects of Semaglutide and adenosine on kidney protein expression in obese mice induced by a high-fat diet (HFD), to identify signaling pathways involved in the obesity-related glomerulonephropathy (ORG) regulation using a proteomics approach.

Materials and methods A total of 48 mice were divided into normal-fat diet (NFD), high-fat diet (HFD), HFD + semaglutide intervention (HS), and HFD + adenosine intervention (HA) groups. Mouse serum, urine, and kidney tissue samples were collected to identify markers for blood glucose lipid metabolism, inflammation, oxidative stress (OS), kidney damage protein, urinary protein/creatinine, and other relevant factors. The kidney pathological changes of mice were observed under light and electron microscope. The differences in total proteins in the kidneys of mice were analyzed using liquid chromatography-tandem mass spectrometry (LC-MS/MS). The proteins with significant differences were selected for bioinformatics and Western Blot (WB) analyses.

Results Semaglutide and adenosine can reduce the weight of obese mice, improve the level of glucose and lipid metabolism, inflammation, and OS in obese mice, and have a positive effect on glomerular and tubular lesions in mice. The TXNIP/NLRP3 signaling pathway, which is involved in the pathogenesis of murine ORG, was screened using a proteomics approach. Western Blot showed that the expressions of Txn, Txnip, and NLRP3 in HFD mice were significantly higher than those of NFD mice, while the expression levels of Txn, Txnip, and NLRP3 in HS and HA mice were substantially lower than those of HFD mice.

Conclusion Semaglutide and adenosine can ameliorate obesity-induced renal injury, potentially through modulation of the Txnip/NLRP3 pathway.

Keywords Obesity, Semaglutide, Adenosine, Obesity-related glomerulonephropathy, Proteomics

*Correspondence:
Shuchun Chen
chenshuc2014@163.com
[1]Department of Internal Medicine, Hebei Medical University, Shijiazhuang, People's Republic of China
[2]Department of Endocrinology, Hebei General Hospital, Shijiazhuang, People's Republic of China
[3]Key Laboratory of Metabolic Diseases in Hebei Province, Shijiazhuang, People's Republic of China
[4]Department of Endocrinology, The Second Affiliated Hospital of Anhui Medical University, Hefei, Anhui, China

Introduction

Obesity is a chronic metabolic disease that significantly affects various clinical domains, particularly endocrinology, cardiology, and nephrology [1]. Currently, body mass index (BMI) is often used to assess obesity, defined as a BMI of ≥ 30 kg/m². In 2020, nearly 1 billion individuals worldwide were classified as obese, and it is expected that this figure will rise to 1.5 billion by 2030 [2]. Obesity poses a significant threat to human health and results in various complications. Studies show that there is a J-shaped relationship (J-shaped relationship refers to a specific nonlinear association pattern where the plotted curve resembles the letter "J." At low exposure levels, the risk decreases as the independent variable increases, but beyond a critical threshold, this trend reverses abruptly) between BMI and patient mortality. In obese patients, BMI is positively related to an increase in the risk of all-cause death [3]. Simultaneously, obesity presents significant obstacles to social medicine. According to the 2018 China Medical Expense Statistics, medical expenses associated with overweight and obesity represented 3.9% of total medical care costs and 4.31% of non-hospitalization expenditures [4].

Obesity-associated glomerular nephropathy (ORG) is a kidney complication caused by obesity. The prevalence of ORG increased by 10 times from 1986 to 2000 [5]. The main manifestations of ORG are proteinuria, glomerular hypertrophy, progressive glomerulosclerosis, and renal dysfunction. A BMI of ≥ 30 kg/m [2] correlates with reduced eGFR and heightened albuminuria in individuals, presenting a relative risk of 1.36 (1.18–1.56) [6]. The etiology of ORG indicates that adipocytes release numerous lipids and inflammatory mediators in obesity, resulting in metabolic dysregulation, inflammation, and insulin resistance (IR), which contribute to glomerular hyperfiltration, damage, and atrophy of kidney units [7]. Systemic chronic low-grade inflammation and localized renal inflammatory injury play pivotal roles in the pathogenesis of obesity-related glomerulopathy (ORG), with the TXNIP/NLRP3 pathway serving as a key mediator in activating inflammatory cascades [5].

Semaglutide is a standard weekly glucagon-like peptide 1 (GLP-1) receptor agonist formulation. It has emerged as a novel class of weight control medicines due to its suppression of the appetite center, which promotes weight reduction [8]. Previous studies have shown that semaglutide can improve the weight loss of obese mice, improve the extent of inflammation and glucose and lipid metabolism, and reverse the kidney damage of obese mice via NAD + metabolism and IR-related metabolic pathways [9]. Adenosine is a drug used in cardiology to treat paroxysmal supraventricular tachycardia; simultaneously, it serves as a crucial endogenous regulator that preserves cellular and tissue homeostasis throughout pathological conditions and stress stimuli [10]. Adenosine interacts with four adenosine receptors (A1, A2a, A2b, A3). A recent study has discovered that adenosine can activate brown fat cells in mice through the A2a receptor, thereby preventing obesity due to a high-fat diet [11]. In our previous renal metabolic histological studies, the adenosine level of obese mice decreased. Treatment of semaglutide in obese mice resulted in an elevation of adenosine levels, semaglutide demonstrated renal protective effects by upregulating adenosine concentrations [9]. To further investigate whether the TXNIP/NLRP3 signaling pathway mediates the renoprotective effects of semaglutide and adenosine in obese mice, this study builds upon prior research by designing a new set of experiments. Using proteomics technology, we identified specific therapeutic targets associated with obesity-related kidney complications.

Materials and methods

Animals, reagents and materials

A total of 48 male C57BL/6J mice, aged 5 weeks, were obtained from SPF Biotechnology Co., Ltd (Beijing, China). F02-002 normal-fat feed (10% total caloric content from fat) and D12492 high-fat feed (60% total caloric content from fat) were purchased from SPF Biotechnology Co., Ltd (Beijing, China). Semaglutide was provided by Novo Nordisk, Denmark. Adenosine was purchased from Medchemexpress (United States). Urine protein (E-BC-K252-M) and urine creatinine (E-BC-K188-M) test kits were purchased from Elabscience Biotechnology Co.,Ltd (Wuhan, China). The total cholesterol (TC), low-density lipoprotein cholesterol (LDL-C) test kits (S03042, S03029) and malondialdehyde (MDA) kits (A003-1) were obtained from Nanjing Construction Bioengineering Research Institute Co., Ltd (Nanjing, China). Tumor necrosis factor-α (TNF-α) kits (MU30030), interleukin-6 (IL-6) kits (MU30044), interleukin-18 (IL-18) kits (MU30380) were purchased from bioswamp (Wuhan, China). The blood glucose meter was Accu-CHEK (American). Anti-Txn antibody(ab53006), Anti-Txnip antibody (ab29687), Anti-Nlrp3 antibody (ab49012) and Anti-β-actin antibody (ab181602) were purchased from Servicebio (Wuhan, China).

Experimental animals and treatment regimen

All animals (5-week-old) were housed in an appropriately controlled animal room (22 ± 2 °C, humidity 55 ± 10%, 12 h light/dark cycle), with regular bedding changes, allowing free access to food and water. After a week of adaptive feeding of ordinary feed, the mice were randomly divided into 4 groups: the normal-fat diet (NFD, $n = 12$), the high-fat feed diet (HFD, $n = 12$), the HFD + semaglutide intervention (HS, $n = 12$), and the HFD + adenosine intervention (HA, $n = 12$). During the

initial 14 weeks, NFD mice were provided standard feed, while HFD, HS, and HA mice received a high-fat diet. After 14 weeks, the feeding methods for the HS and HA groups remained similar; however, the HS group received daily intraperitoneal injections of 30 nmol/kg/d semaglutide, while the HA group received 20 mg/kg/d adenosine daily via the same intraperitoneal injections. The method and dosage of administration refer to the research of other researchers [9, 12]. The diet of mice in the NFD and HFD groups remained unchanged, and they were injected with equal volumes of saline every day. Feeding was continuously provided for 8 weeks after difference intervention, with a total intervention time of 22 weeks. The body weight of mice from all groups was measured every week (Fig. 1).

Glucose tolerance tests

Before the end of the experiment, blood glucose levels of mice were monitored using blood glucose meter. The fasting blood sugar of the mouse was measured after a 12-hour fast, and then 20% high glucose (2 g/kg) was administered to the abdominal cavity. After injecting high sugar, blood sugar was measured and recorded by collecting mouse tail vein blood at different time points: 15, 30, 60, 90, and 120 min. The intraperitoneal glucose tolerance test (IPGTT) area under the curve (AUC) was computed. B = 0.5 * (Bg 0 min + Bg 30 min)/2 + 0.5 * (Bg 30 min + Bg 60 min)/2 + 1 * (Bg 60 min + Bg 120 min)/2, IPGTT AUC = 0.5, B Glucose was the blood sugar value at each point in time.

Sample collection and metabolic analyses

Mouse urine was collected in a metabolic cage after 22 weeks of intervention. The upper liquid (supernatant) was extracted after centrifugation at 2000 rpm for 10 min. The enzyme-linked immunosorbent assay (ELISA) kits were used to measure the protein and creatinine content in the urine of mice. After a 12 h fast, mice were anesthetized with 1% pentobarbital sodium (60 mg/kg) via the abdominal cavity route. Blood was drawn from the inner canthus vein. Immediately after blood collection, the mouse was euthanized via cervical dislocations. These blood samples were allowed to rest for 60 min, then centrifuged (4 ℃, 3500 rpm, 15 min), The serum samples were transferred to anticoagulation tubes and the serum total cholesterol (TC), low-density lipoprotein cholesterol (LDL-C) were measured using a fully automated biochemical analyzer. ELISA was used to detect the levels of serum MDA. All procedures were conducted in complete compliance with the manufacturer's directions.

Evaluation of inflammatory and oxidative stress markers in kidney tissues

Bilateral kidneys were harvested from the mouse's abdominal cavity during dissection and were promptly

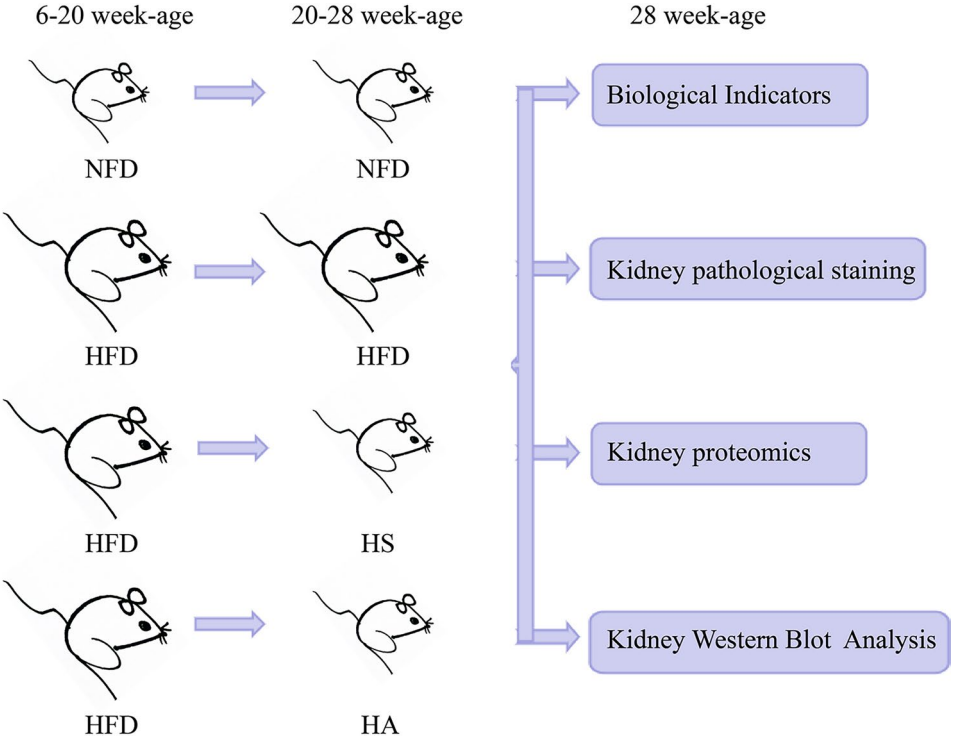

Fig. 1 Experimental flow chart. Abbreviations: NFD, normal-fat diet; HFD, high-fat die; HS, HFD + semaglutide intervention; HA, HFD + adenosine intervention

stored in a -80 °C refrigerator. Three left kidney samples were randomly selected from each group. The renal tissue was lysed using protein lysate and centrifuged for 15 min at 4 ℃ and 3000 rpm. The mediators, including TNF-α, IL-18, and IL-6, were quantified in the kidney tissues using the ELISA method. All procedures were performed under the strict guidelines of manufacturers.

Histopathological examination of kidney tissues

Three left kidney samples were randomly selected for each group and fixed in 4% paraformaldehyde (PFA) for 48 h at room temperature. After fixation, tissues were processed in a graded series of alcohol dehydration, xylene clearing, embedded in paraffin, and sectioned into 5 μm thickness. Histopathological changes in the kidneys were analyzed using H&E staining, periodic acid-Schiff (PAS), and Masson's trichrome staining. Approximately 10 random fields per group were selected for analysis of glomerular diameter via HE staining and glomerular area using PAS (glycogen) staining. Next, renal tubular injury was assessed in 10 different fields per group. Tubular damage was characterized by brush border loss, tubular swelling or atrophy, and tubular casts. Renal tubular damage was evaluated as per the percentage of injured tubules in each field of view: 0 points for no damage, 1 point for < 25% damage, 2 points for 25–50% damage, 3 points for 50–75% damage, and 4 points for 75–100% damage [9]. From each group, 10 random fields were selected to determine the positive staining area as a percentage of the total area under Masson trichrome staining. The percentage of renal interstitial fibrosis area was calculated using the following formula: percentage of renal interstitial fibrosis area (%) = collagen pixel area/tissue pixel area × 100%.

Kidney tissue was preserved in 4% PFA, sectioned to a thickness of 5 μm, and stained with Oil Red O solution. After washing with PBS (thrice), nuclei were counterstained with hematoxylin to elucidate renal lipid accumulation. For quantitative analysis, 10 random fields of view were selected from each group to measure the Oil Red O-positive area ratio (calculated as: positive area / total tissue area).

Selected the observation field of view as ×400 magnification. Data analysis was performed using Image-Pro Plus software.

Transmission electron microscopy (TEM)

From each animal, three 1 mm^3 cortical fragments were randomly sampled from the left kidney, immersion-fixed in 2.5% glutaraldehyde (in 0.1 M PBS, pH 7.4) at 4 °C for 24 h. Rinse with 0.1 M phosphate buffer 3 times. Then used 1% osmium acid room temperature to fix for 2 h. After gradient alcohol dehydrated, the tissues were infiltrated by a 1:1 solution of anhydrous acetone and an embedding agent. Ultrathin sections (80 nm) were prepared on copper grids and stained with tannic acid and lead solution. Observation with a transmission electron microscope. For each group, five random fields were selected, with two random measurements of glomerular basement membrane (GBM) thickness performed per field. Each measurement was taken from the endothelial cell layer to the epithelial cell layer. Subsequently, five random fields were selected per group, and two podocyte foot process width measurements were performed in each field. Data analysis was performed using Image-Pro Plus software.

Sample preparation for protein isolation

Three left kidney samples per group (20–50 mg wet weight each) were lysed in 1 mM protease and phosphatase inhibitor cocktail, pH 8.5, and incubated at 99 °C for 30 min. after cooling to room temperature, trypsin (Promega, Madison, WI, USA, #V5280) was added and the samples were digested for 18 h at 37 °C. 10% formic acid was added and vortex for 3 min, followed by sedimentation for 5 min (12,000 g). Next, a new 1.5 mL tube with extraction buffer (0.1% formic acid in 50% acetonitrile) was used to extract the supernatant (vortex for 3 min, followed by 12,000 g of sedimentation for 5 min). Collected supernatant and dried using a speed-vac. 20 μg protein for each sample were mixed with 2X loading buffer respectively and boiled for 5 min. The proteins were separated on SDS-PAGE gel (constant current 120 V, 60 min). Protein bands were visualized by Coomassie Blue R-250 staining.

Nano-LC–MS/MS analysis

For the proteome profiling samples, peptides were analyzed on a timsTOF Pro mass spectrometer (Bruker) coupled with a high-performance liquid chromatography system (nanoElute 2, Bruker). Dried peptide samples redissolved in Solvent A (0.1% formic acid in water) were loaded onto a 2-cm self-packed trap column (100 μm inner diameter, 3 μm ReproSil-Pur C18-AQ beads, Dr Maisch GmbH) using Solvent A and separated on a 150 μm-inner-diameter column with a length of 30 cm (1.9 μm ReproSil-Pur C18-AQ beads, Dr Maisch GmbH) over a 150 min gradient (Solvent A: 0.1% formic acid in water; Solvent B: 0.1% formic acid in 80% ACN) at a constant flow rate of 600 nL/min (0–150 min, 0 min, 4% B; 0–10 min, 4-15% B; 10–125 min, 15-30% B; 125–140 min, 30-50% B; 140–141 min, 50-100% B; 141–150 min, 100% B). After separation by chromatography, the samples were analyzed using a timsTOF Pro 2 mass spectrometer. The detection mode was positive ionization, with the ion source voltage set to 1.6 kV. Both MS and MS/MS analyses were performed using time-of-flight (TOF) detection. The mass spectrometry scan range was set from 100 to

1700 m/z. The 1/K0 Start was set to 0.85 Vs/cm^2, and the 1/K0 End was also set to 0.85 Vs/cm^2. The ion accumulation and Rapm times were both set to 100 ms. Data acquisition was conducted in Parallel Accumulation Serial Fragmentation (PASEF) mode, with four PASEF mode fragment ion collections following each primary MS spectrum acquisition. A cycle window time of 0.53 s was employed. Secondary spectra within the charge range of 0–5 were obtained, with a dynamic exclusion time of 24 s set for the tandem mass spectrometry scans to avoid redundant scanning of fragment ions.

Data analysis

The original data of mass spectrometry analysis were. d files, and MaxQuant was used for qualitative and quantitative analysis. The screening criterion for qualitative data analysis was set at a peptide false discovery rate (FDR) of ≤ 0.01.

GO and KEGG analyses

Proteins with an absolute log2 fold change (log2FC) ≥ 1 and a p-value < 0.05 were screened, and Gene Ontology (GO) functional enrichment analysis (http://www.ebi.ac.uk/goa/) and Kyoto Encyclopedia of Genes and Genomes (KEGG) pathway enrichment analysis (https://www.kegg.jp/kegg/mapper/) were conducted on the selected differentially expressed proteins (DEPs). Fisher's exact test was used to validate the enrichment analysis, with differences considered statistically significant at $p < 0.05$.

Construction of PPI network

DEPs from the HFD/NFD, HS/HFD, and HA/HFD groups were imported to the STRING (http://www.string-db.org) online database. An interaction score of ≥ 0.15 was set to define protein-protein interactions (PPI). The resulting data were then visualized using Cytoscape software. The degree algorithm was applied to identify the top 10 DEPs with the most potent interaction to find proteins related to the pathogenesis of ORG.

Key proteins and pathways identification via WB

Kidney tissues (50 mg) from three mice per group were processed for protein extraction in 500 μL RIPA lysis buffer and 5 μL protease inhibitor PMSF. After tissue grinding and centrifugation, supernatants were collected, and total protein concentrations were measured via BCA assay. Samples were loaded on SDS-PAGE comprising 10% polyacrylamide gels (lower layer) and 5% gels (upper layer). The separated proteins were transferred onto PVDF membranes. Membranes were blocked with 5% skim milk for 2 h at room temperature and the antibodies corresponding to NLRP3, Txnip and Txn were added. The Txn antibody (Catalog No.: ab53006, host species: rabbit) was used at a dilution ratio of 1:1000. The Txnip antibody (Catalog No.: ab29687, host species: rabbit) was used at a dilution ratio of 1:1000. The NLRP3 antibody (Catalog No.: ab29687, host species: rabbit) was used at a dilution ratio of 1:1000. Rabbit anti-mouse was selected as the antibody and 4℃ incubated overnight. The HRP-labeled goat anti-rabbit IgG was selected as the secondary antibody and incubated at room temperature for 1.5 h. After adding the Western Lightning™ Chemiluminescence Reagent, the membrane was visualized using an Epson Perfection V39 scanner to measure protein band intensities. The relative intensity of each protein band was calculated by normalizing to the corresponding internal control band, yielding corrected values. These values were then standardized to the control group (as the standard value 1), and a histogram was plotted to display the results.

Statistical analysis

Statistical analyses were performed using SPSS 21.0 software, and graphical data representations were created using GraphPad Prism 8.0.2 and the Micro-ShengXin online tool (https://www.bioinformatics.com.cn). The results were presented as mean ± standard deviation. One-way ANOVA was used for statistical analysis, and the LSD-t test was used for multiple comparisons. Differences with a $p < 0.05$ were deemed statistically significant.

Results

Effect of semaglutide and adenosine on body weight reduction in obese mice

There were no significant differences in the body weight of all groups of mice at the age of 6 weeks. After 14 weeks of high-fat intervention, the body weights of HFD, HS, and HA mice were significantly higher than those of NFD mice ($p < 0.001$), confirming the efficacy of the obesity model. After that, the HS group received semaglutide, while the HA group was administered adenosine. At the end of the experiment, the body weight of HS group mice was significantly lower compared to HFD group mice ($p < 0.001$), and similarly, the body weight of HA group mice was also significantly reduced relative to HFD group mice ($p = 0.044$) (Fig. 2A-B).

Effects of semaglutide and adenosine on glucose and lipid metabolism, kidney damage, inflammation, and oxidative stress in mice

Changes in glucose and lipid metabolism in mice

The glucose tolerance test showed that the blood sugar of HFD mice was higher than that of other groups at respective time points (30, 60, 90, and 120 min) (Fig. 3A). Quantitative analysis revealed that the IPGTT AUC of HFD mice was significantly higher than that of NFD mice ($p < 0.001$), while the IPGTT AUC of HS mice was considerably lower than that of HFD mice ($p < 0.001$).

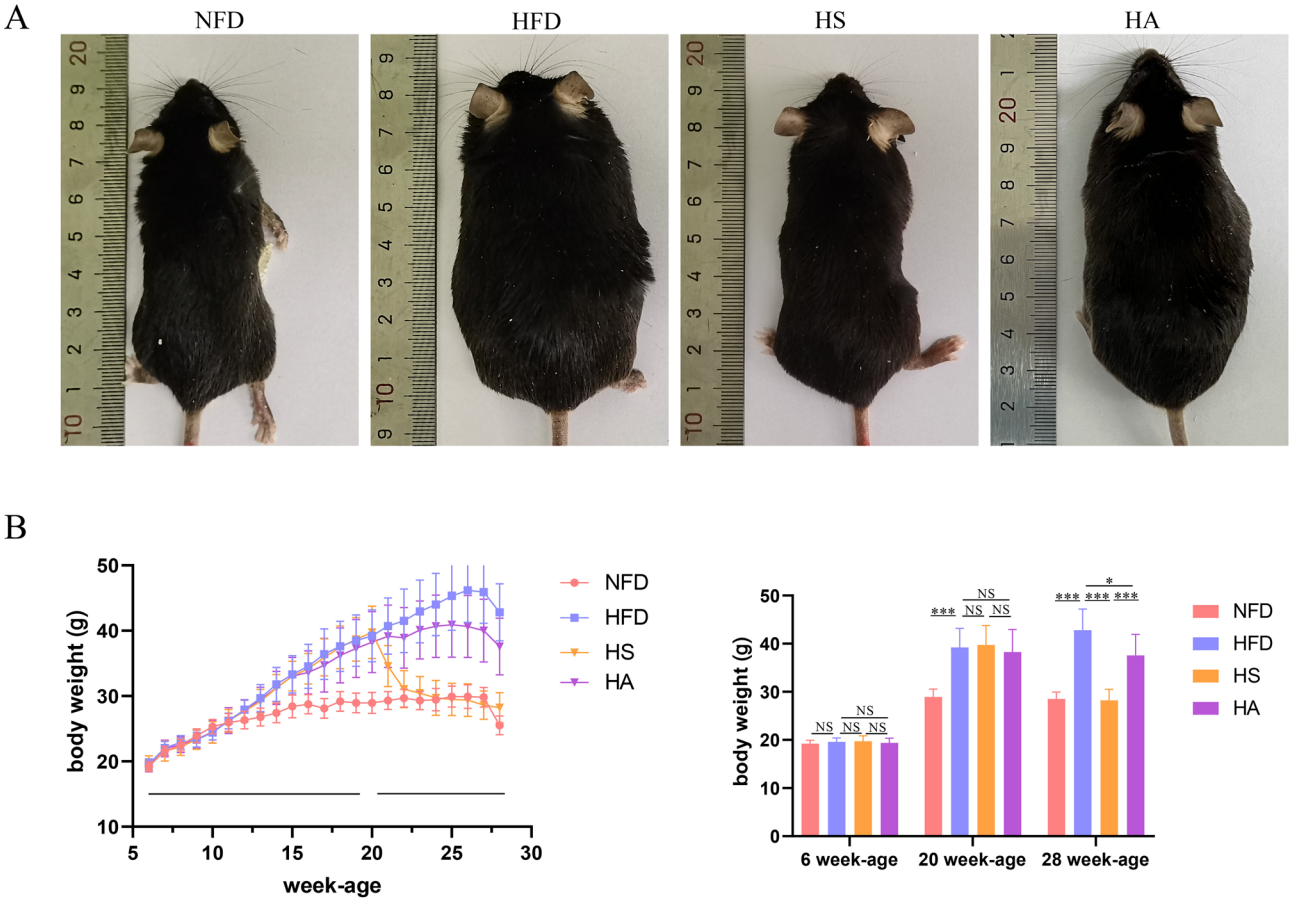

Fig. 2 Weight changes in mice. Images of NFD mice, HFD mice, HS mice and HA mice (**A**); Trends in body weight of mice in NFD, HFD, HS and HA groups, quantitative analysis, $n = 12$ (**B**). Note: *Denotes significance at a P value of < 0.05, **Denotes significance at a P value of < 0.01, ***Denotes significance at a P value of < 0.001, NS indicates that the difference is not statistically significant. Abbreviations: NFD, normal-fat diet; HFD, high-fat die; HS, HFD + semaglutide intervention; HA, HFD + adenosine intervention

The IPGTT AUC of HA mice displayed a downward trend relative to that of HFD mice, but the difference was not statistically significant ($p = 0.268$) (Fig. 3B). Compared with NFD mice, HFD mice showed significantly increased TC levels ($p < 0.001$). Compared with HFD mice, the HS group showed significantly lower TC levels ($p = 0.002$), and the HA group similarly exhibited significant TC reduction ($p = 0.032$) (Fig. 3C). Compared with NFD mice, HFD mice showed significantly increased LDL-C levels ($p = 0.025$). Compared with HFD mice, the HS group showed significantly lower LDL-C levels ($p = 0.02$), and the HA group similarly exhibited significant LDL-C reduction ($p = 0.017$) (Fig. 3D).

Changes in kidney injury in mice

The concentrations of urine protein and urinary creatinine in mice were measured, followed by estimating the urinary protein/creatinine ratio (UACR). The UACR level in HFD mice was significantly elevated compared to NFD mice ($p < 0.001$). In contrast, the UACR levels in HS mice was dramatically reduced relative to the HFD group ($p < 0.001$), the UACR levels in HA mice was dramatically reduced relative to the HFD group ($p = 0.001$) (Fig. 3E).

Changes in the level of inflammation and oxidative stress in mice

The serum MDA level of HFD mice was significantly higher than that of NFD mice ($p = 0.001$), the serum MDA level of HS mice was considerably lower than that of HFD mice ($p = 0.003$), the serum MDA level of HA mice was considerably lower than that of HFD mice ($p = 0.042$) (Fig. 3F). The levels of TNF-α, IL-6, and IL-18 in the kidney tissue of HFD mice were significantly higher than those of NFD mice ($p < 0.001$), the levels of TNF-α, IL-6, and IL-18 in HS mice substantially lower than those of HFD mice ($p = 0.044$, $p < 0.001$, $p = 0.01$, respectively), the levels of TNF-α, IL-6, and IL-18 in HA mice substantially lower than those of HFD mice ($p < 0.001$, $p = 0.06$, $p = 0.01$, respectively) (Fig. 3G-I).

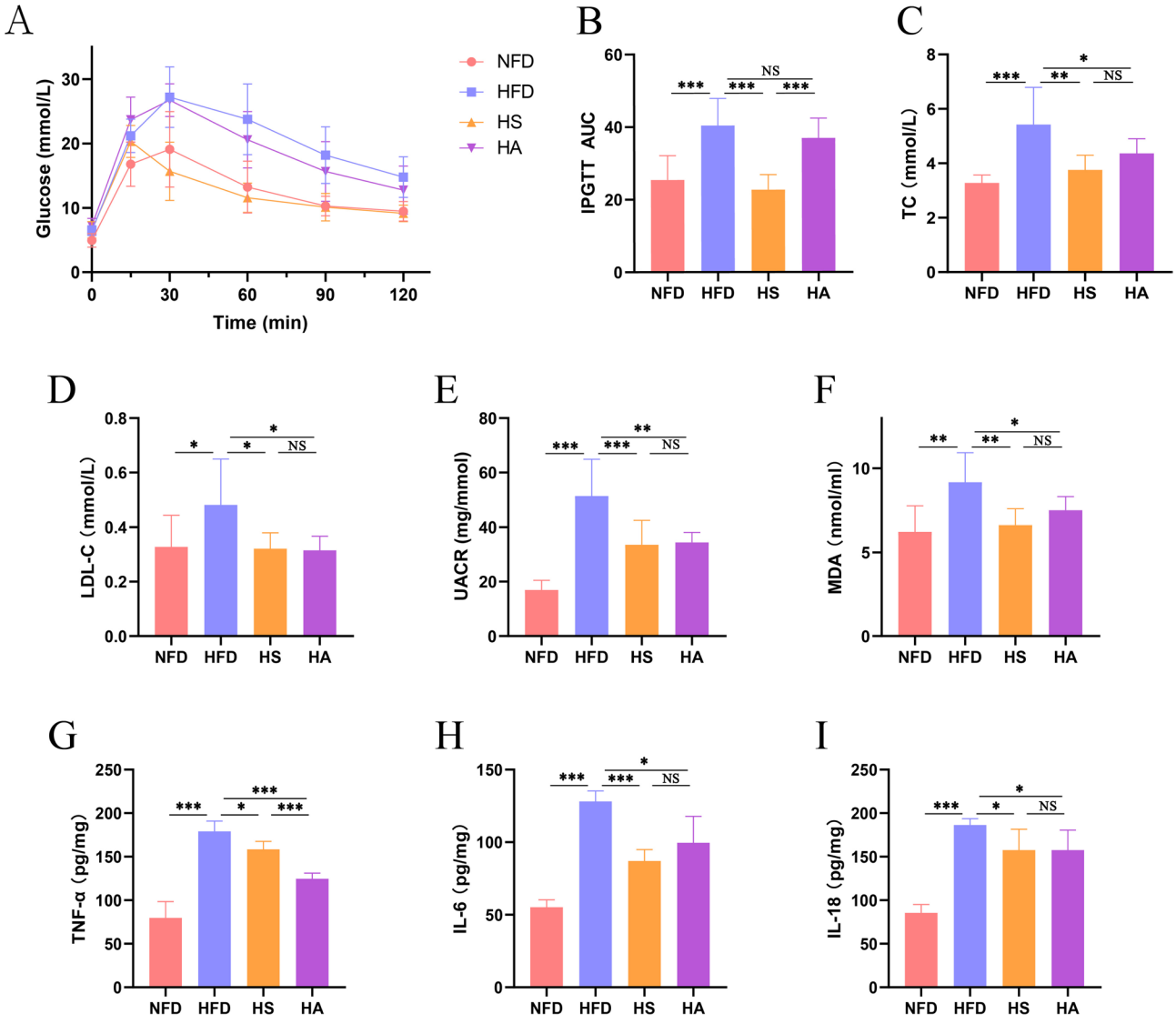

Fig. 3 Changes in glucose and lipid metabolism, kidney injury, inflammation and oxidative stress in mice. Changes of Glucose, quantitative analysis, $n=8$ (**A**), IPGTT AUC, quantitative analysis, $n=8$ (**B**), TC, quantitative analysis, $n=3$, repeat 2 experiments (**C**), LDL-C, quantitative analysis, $n=3$, repeat 2 experiments (**D**), UACR, quantitative analysis, $n=8$ (**E**), MDA, quantitative analysis, $n=3$, repeat 2 experiments (**F**), TNF-α, quantitative analysis, $n=3$, repeat 2 experiments (**G**), IL-6, quantitative analysis, $n=3$, repeat 2 experiments (**H**) and IL-18, quantitative analysis, $n=3$, repeat 2 experiments (**I**). Note: *Denotes significance at a P value of < 0.05, **Denotes significance at a P value of < 0.01, ***Denotes significance at a P value of < 0.001, NS indicates that the difference is not statistically significant. Abbreviations: NFD, normal-fat diet; HFD, high-fat die; HS, HFD + semaglutide intervention; HA, HFD + adenosine intervention; IPGTT, intraperitoneal glucose tolerance test; TC, total cholesterol; LDL-C, low-density lipoprotein cholesterol; UACR, urinary protein/creatinine; MDA, malondialdehyde; TNF-α, tumor necrosis factor-α; IL-6, interleukin-6; IL-18, interleukin-18

Effect of semaglutide and adenosine on kidney pathological changes

Weight of mouse's left kidney

Macroscopic observation revealed that the left kidneys of HFD-fed mice appeared enlarged in size compared to those in other groups (Fig. 4A). Based on the correlation analysis, the left kidney weight of mice has a positive correlation with weight ($r=0.68$) (Fig. 6A).

H&E staining

Histology of kidney sections indicated that the glomerular matrix in HFD mice was mildly more proliferative than in NFD mice, with pronounced vacuolar degeneration, cell swelling, and visible brush border loss in renal tubular epithelial cells. Glomerular and tubular lesions were less severe in HS and HA mice compared to HFD mice (Fig. 4B). Quantitative analysis demonstrated that the glomerular diameter in HFD mice was significantly larger than in NFD mice ($p=0.001$). In contrast, HS and HA mice had significantly reduced glomerular diameters

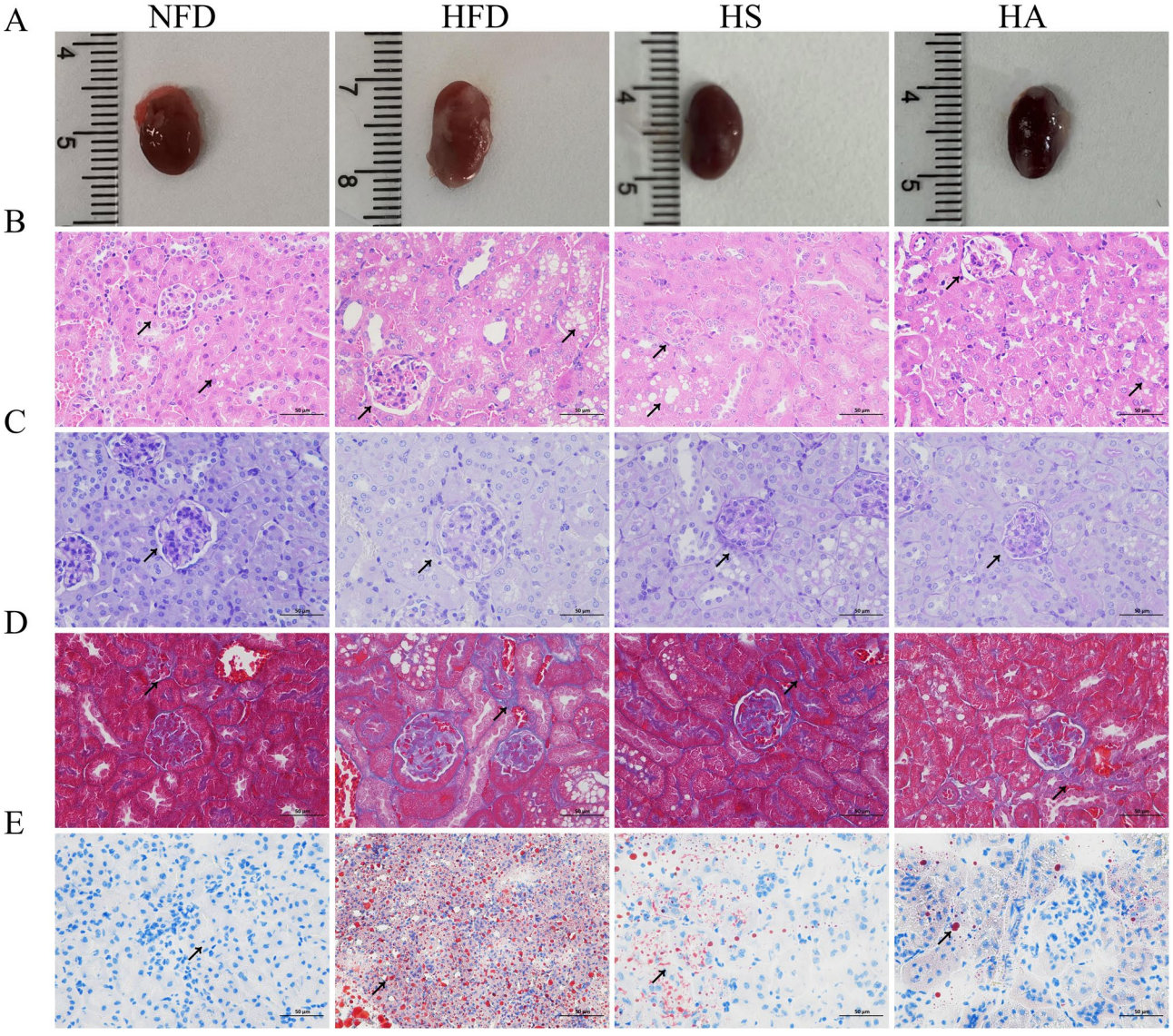

Fig. 4 Macroscopic and light microscopic changes in the mouse kidney. Images of NFD mice kidney, HFD mice kidney, HS mice kidney and HA mice kidney (**A**); H&E staining of kidneys, qualitative analysis, $n = 10$ (**B**); PAS staining of kidneys, qualitative analysis, $n = 10$ (**C**); Masson trichrome staining of kidneys, qualitative analysis, $n = 10$ (**D**), and oil red O staining of kidneys, qualitative analysis, $n = 10$ (**E**). The arrow indicates the lesion site. Abbreviations: NFD, normal-fat diet; HFD, high-fat die; HS, HFD + semaglutide intervention; HA, HFD + adenosine intervention

compared to HFD mice ($p = 0.003$, $p = 0.004$, respectively) (Fig. 6B). The renal tubular injury index was significantly higher in HFD mice than in NFD mice ($p < 0.001$); HS and HA mice showed a trend toward lower injury indices. However, this difference was not statistically significant ($p = 0.119$, $p = 0.119$, respectively) (Fig. 6D).

PAS staining

The glomerular area of HFD mice was substantially larger than that of NFD mice, and the glomerular mesangial cells showed hyperplasia, as observed by PAS staining. In contrast, the glomerular HS mice and HA mice showed no apparent abnormalities (Fig. 4C). Quantitative analysis revealed that the glomerular area of HFD mice was considerably larger than that of NFD mice ($p = 0.001$). In comparison, the glomerular area of HS and HA mice was significantly smaller than that of HFD mice ($p = 0.001$, $p = 0.002$, respectively) (Fig. 6C).

Masson trichrome staining

Masson trichrome staining revealed considerable renal interstitial fibrosis in HFD mice, while HS and HA mice showed markedly less renal interstitial fibrosis (Fig. 4D). The percentage of interstitial fibrosis area in HFD mice was markedly greater than in NFD mice ($p < 0.001$). In contrast, the percentage of renal interstitial fibrosis area in HS and HA mice was significantly lower than in HFD

mice, with a statistically significant difference ($p < 0.001$, $p < 0.001$, respectively) (Fig. 6E).

Oil red O staining

The light microscope revealed that lipid deposition was more apparent in HFD mice than in NFD mice ($p < 0.001$). Conversely, HS mice and HA mice showed less lipid deposition than HFD mice ($p < 0.001$, $p < 0.001$, respectively) (Figs. 4E and 6F).

Transmission electron microscopy

Transmission electron microscopy (TEM) revealed that the damage to glomerular endothelial cells in HFD mice was remarkably pronounced, showing membrane damage, matrix dissolution, vacuolar degeneration, organelle disintegration, and increased fusion of foot processes. In contrast, the ultrastructural damage observed in HS and HA mice podocytes was less severe than that in HFD mice, characterized by intact basal membranes and reduced organelle swelling (Fig. 5). Quantitative analysis indicated that both the GBM and the width of podocyte foot process in HFD mice were significantly greater than those in NFD mice ($p < 0.001$). In contrast, both the GBM and podocyte foot process width were significantly reduced in HS mice compared to HFD mice ($p < 0.001$, $p < 0.001$, respectively), both the GBM and podocyte foot process width were significantly reduced in HA mice compared to HFD mice ($p < 0.001$, $p = 0.001$, respectively) (Fig. 6G-H).

Kidney proteomics analysis of mice

Identification of differential expression proteins in mice

A total of 223 DEPs were identified in the kidney tissue of the HFD/NFD group, with 62 upregulated proteins and 161 downregulated proteins as per the DEPs screening criteria. In the kidney tissue of the HS/HFD group, a total of 715 DEPs were identified, of which 87 protein expression was reduced, and 628 protein expression was upregulated. The kidney tissue of the HA/HFD group contained a total of 859 DEPs, of which 115 protein expressions were reduced and 744 protein expressions were enhanced. Differential expression analysis and significant differential protein clustering analysis of DEPs are illustrated with heat maps and volcanic maps (Fig. 7A-B).

GO and KEGG enrichment analysis of deps

A total of 223 DEPs were found in the kidney tissue of the HFD/NFD group, comprising 62 upregulated and 161 downregulated. GO functional enrichment analysis of the 62 upregulated DEPs revealed their involvement in several biological processes (BP), such as cellular lipid metabolic processes, actin filament organization, negative regulation of protein modification, positive regulation of apoptosis, and amide metabolism. Considering molecular function (MF), the DEPs were associated with cytoskeletal protein binding, actin binding, acyltransferase activity, GTPase binding, and guanyl nucleotide binding. For cellular components (CC), the DEPs were predominantly localized in the cytoskeleton, nuclear body, nuclear speck, microtubules, and midbody. KEGG enrichment analysis shows that DEPs were mainly enriched in the PPAR signaling pathway, Valine, leucine,

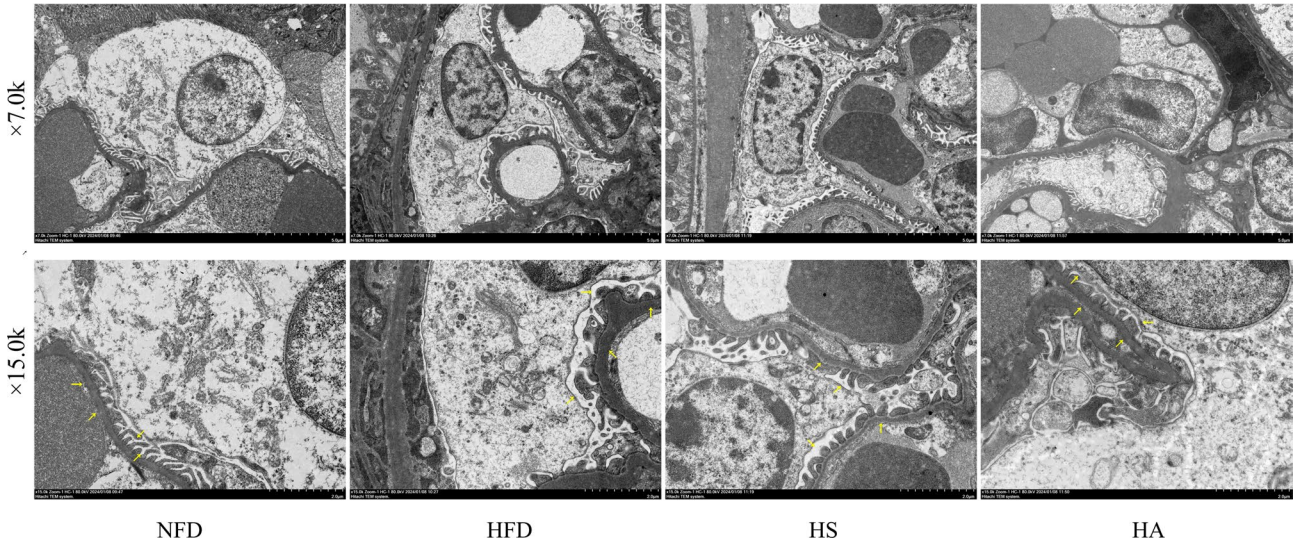

Fig. 5 Electron microscopic findings of renal pathology in mice. Ultrastructural images of NFD, HFD, HS, and HA mice kidneys under an electron microscope, with quantitative analysis, $n = 10$. The arrow indicates the lesion site. Abbreviations: NFD, normal-fat diet; HFD, high-fat die; HS, HFD + semaglutide intervention; HA, HFD + adenosine intervention

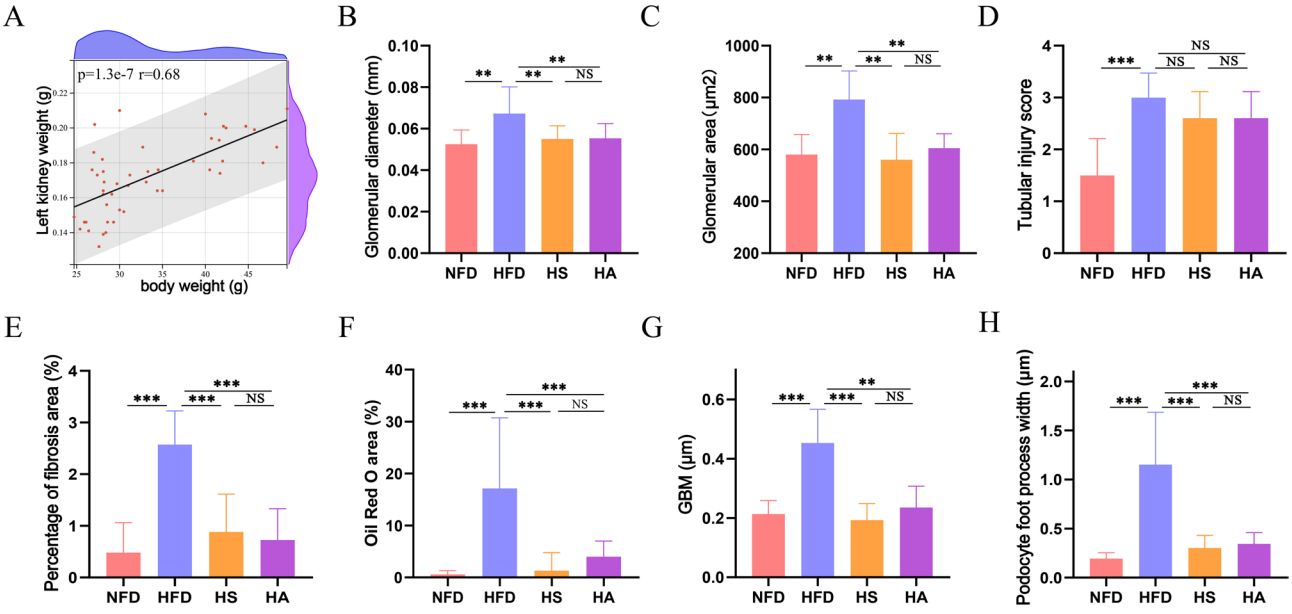

Fig. 6 Quantitative analysis of renal pathological changes in mice. Correlation between left kidney weight and weight, $n=12$ (**A**); Changes of glomerular diameter, quantitative analysis, $n=3$, repeat 10 experiments (**B**); Changes of glomerular area, quantitative analysis, $n=3$, repeat 10 experiments (**C**); Changes of tubular injury score, quantitative analysis, $n=3$, repeat 10 experiments (**D**); Changes of percentage of fibrosis area, quantitative analysis, $n=3$, repeat 10 experiments (**E**); Changes of Oil Red O area, quantitative analysis, $n=3$, repeat 10 experiments (**F**); Changes of GBM, quantitative analysis, $n=3$, repeat 10 experiments (**G**); Changes of podocyte foot process width, quantitative analysis, $n=3$, repeat 10 experiments (**H**). Note: *Denotes significance at a P value of <0.05, **Denotes significance at a P value of <0.01, ***Denotes significance at a P value of <0.001, NS indicates that the difference is not statistically significant. Abbreviations: GBM, Glomerular Basement Membrane

and isoleucine degradation, Fatty acid degradation, Retinol metabolism, and Pyruvate metabolism (Fig. 8A). The GO function enrichment analysis of downregulated 161 DEPs demonstrates that these proteins were primarily involved in the carboxylic acid metabolic process, oxoacid metabolic process, organonitrogen compound biosynthetic process, carbohydrate derivative metabolic process, and nucleoside phosphate metabolic process in terms of BP. Regarding MF, DEPs were related to oxidoreductase activity, active transmembrane transporter activity, phosphatase activity, carbohydrate binding, and lipid binding. On cell components (CC), DEPs were mainly distributed in the mitochondrial membrane, intracellular organelle lumen, apical plasma membrane, mitochondrial inner membrane, and organelle inner membrane. The KEGG enrichment analysis indicates that DEPs were primarily enriched in the following pathways: Metabolic pathways, Other glycan degradation, Valine, leucine, and isoleucine degradation, Propanoate metabolism, and Glyoxylate and dicarboxylate metabolism (Fig. 8B).

A total of 715 DEPs were identified in the kidney tissue of the HS/HFD group, of which 628 proteins were upregulated and 87 proteins were downregulated. The GO function enrichment analysis of 628 overexpressed DEPs showed that in terms of BP, DEPs were mainly involved in the macromolecule catabolic process, cytoskeleton organization, carboxylic acid metabolic process, carbohydrate derivative metabolic process, regulation of amide metabolic process. Regarding MF, DEPs were related to cytoskeletal protein binding, protein domain-specific binding, DNA-binding transcription factor binding, GTPase activator activity, and lipase activity. On CC, DEPs were mainly distributed in the ribonucleoprotein complex, mitochondrial membrane, cytoskeleton, transferase complex, and organelle inner membrane. KEGG enrichment analysis showed that DEPs were primarily enriched in the mRNA surveillance pathway, nucleocytoplasmic transport, ErbB signaling pathway, ATP-dependent chromatin remodeling, Ubiquinone, and another terpenoid-quinone biosynthesis (Fig. 9A). Analysis of the GO function enrichment of 87 downregulated DEPs showed that in terms of BP, DEPs were mainly involved in the amide metabolic process, cellular lipid metabolic process, regulation of intracellular transport, actin cytoskeleton organization, and regulation of organic acid transport. In terms of MF, DEPs were related to oxidoreductase activity, ribonucleoside triphosphate phosphatase activity, kinase regulator activity, GTPase activity, and scaffold protein binding. On CC, DEPs were mainly distributed in the ribonucleoprotein complex, mitochondrial inner membrane, organelle inner membrane, vesicle membrane, and cytoskeleton. KEGG enrichment analysis demonstrated that DEPs were primarily enriched in Vasopressin-regulated water reabsorption, retinol metabolism, vascular smooth muscle contraction, endocrine

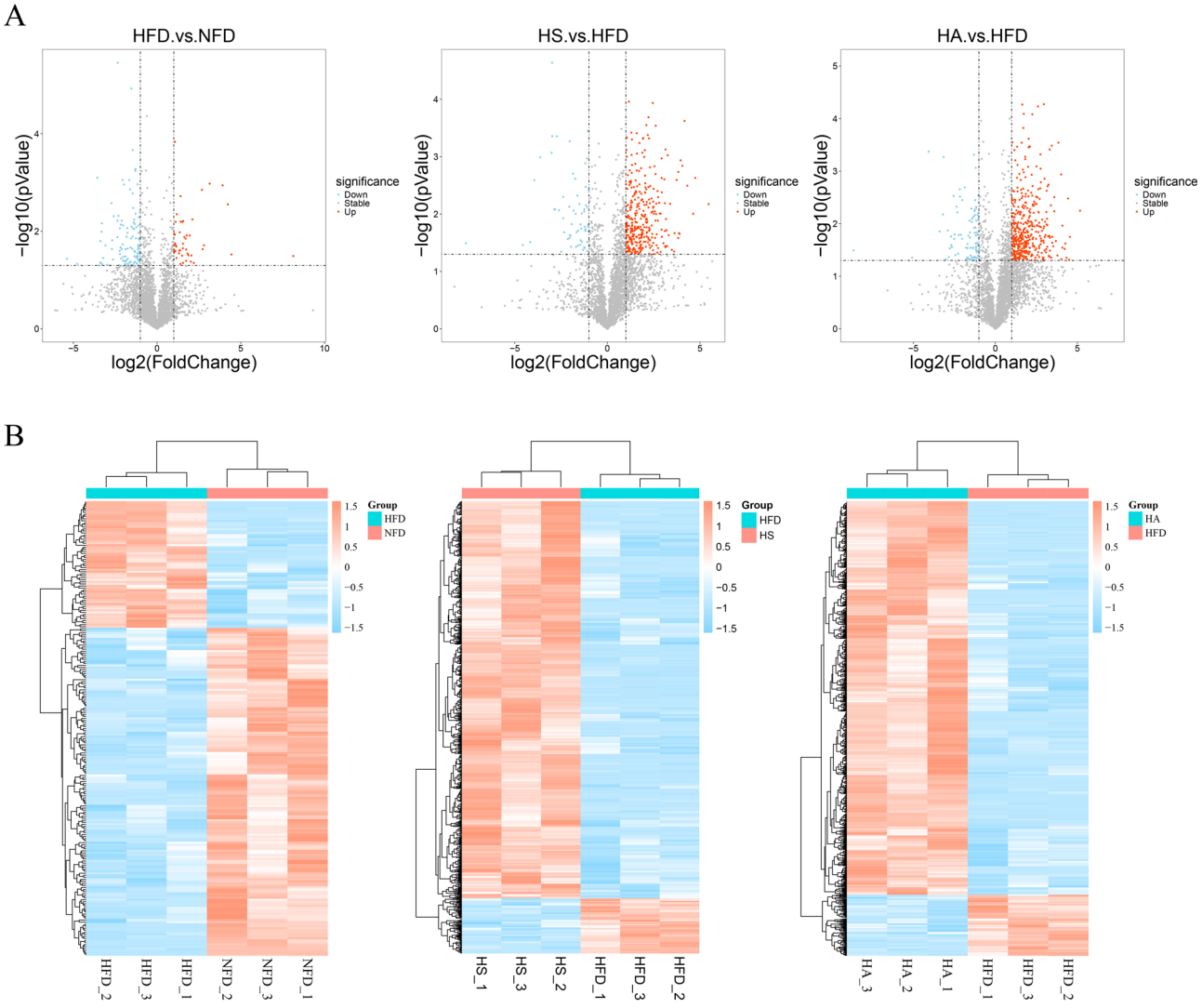

Fig. 7 Identification of mice kidney proteomics DEPs. Volcano map analysis of DEPs (**A**); Cluster heat map analysis of DEPs (**B**). Abbreviations: NFD, normal-fat diet; HFD, high-fat die; HS, HFD + semaglutide intervention; HA, HFD + adenosine intervention

and other factor-regulated calcium reabsorption, glycolysis/gluconeogenesis (Fig. 9B).

A total of 859 DEPs were identified in the kidney tissue of the HA/HFD group, of which 744 proteins were enhanced and 115 proteins were reduced. The GO function enrichment analysis of 744 overexpressed DEPs revealed that DEPs were primarily involved in the carboxylic acid metabolic process, intracellular protein transport, carbohydrate derivative metabolic process, cellular lipid metabolic process, and negative regulation of apoptotic process in terms of BP. In terms of MF, DEPs were associated with pyrophosphatase activity, cytoskeletal protein binding, protein domain-specific binding, oxidoreductase activity, and GTPase binding. On cell components (CC), DEPs were mainly distributed in the ribonucleoprotein complex, nucleolus, mitochondrial membrane, cytoskeleton, and organelle inner membrane. KEGG enrichment analysis showed that DEPs were primarily enriched in metabolic, insulin signaling pathways, AMPK signaling pathways, glucagon signaling pathways, and Sphingolipid metabolism (Fig. 10A). Analysis of the GO function enrichment of 115 downregulated DEPs showed that in terms of BP, DEPs were mainly involved in organonitrogen compound biosynthetic process, amide metabolic process, cell death, response to endoplasmic reticulum stress, regulation of NLRP3 inflammasome complex assembly. Regarding MF, DEPs were related to cytoskeletal protein binding, protein domain-specific binding, GTP binding, amide binding, and heat shock protein binding. In terms of CC, DEPs were mainly distributed in ribonucleoprotein complex, mitochondrial membrane, polymeric cytoskeletal fiber, organelle inner membrane, and vesicle membrane. KEGG enrichment analysis demonstrated that DEPs were primarily enriched

A

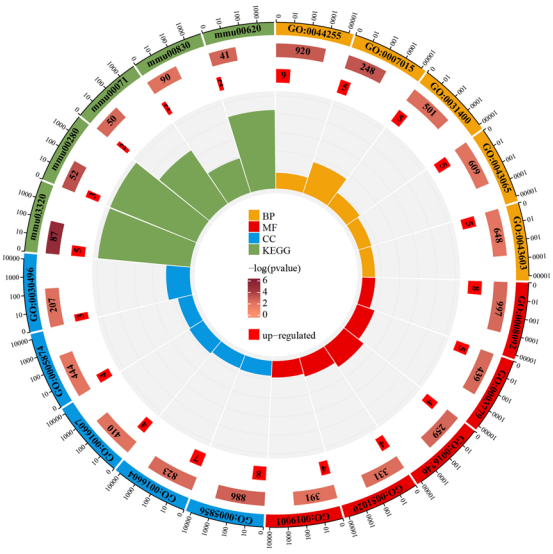

Up−regulated DEPs in HFD/NFD

BP	GO:0044255	cellular lipid metabolic process
BP	GO:0007015	actin filament organization
BP	GO:0031400	negative regulation of protein modification process
BP	GO:0043065	positive regulation of apoptotic process
BP	GO:0043603	amide metabolic process
MF	GO:0008092	cytoskeletal protein binding
MF	GO:0003779	actin binding
MF	GO:0016746	acyltransferase activity
MF	GO:0051020	GTPase binding
MF	GO:0019001	guanyl nucleotide binding
CC	GO:0005856	cytoskeleton
CC	GO:0016604	nuclear body
CC	GO:0016607	nuclear speck
CC	GO:0005874	microtubule
CC	GO:0030496	midbody
KEGG	mmu03320	PPAR signaling pathway
KEGG	mmu00280	Valine, leucine and isoleucine degradation
KEGG	mmu00071	Fatty acid degradation
KEGG	mmu00830	Retinol metabolism
KEGG	mmu00620	Pyruvate metabolism

B

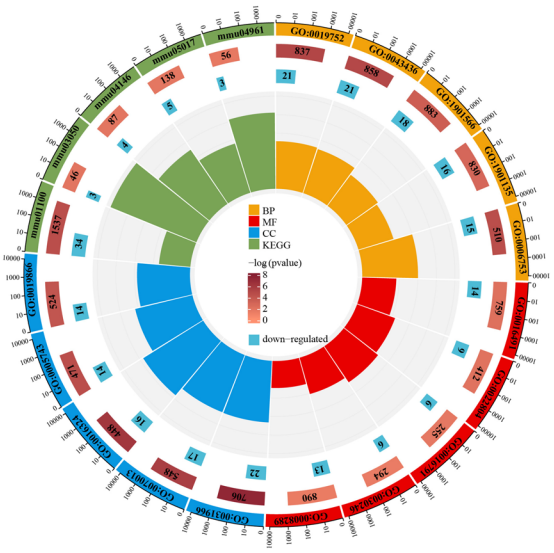

Down−regulated DEPs in HFD/NFD

BP	GO:0019752	carboxylic acid metabolic process
BP	GO:0043436	oxoacid metabolic process
BP	GO:1901566	organonitrogen compound biosynthetic process
BP	GO:1901135	carbohydrate derivative metabolic process
BP	GO:0006753	nucleoside phosphate metabolic process
MF	GO:0016491	oxidoreductase activity
MF	GO:0022804	active transmembrane transporter activity
MF	GO:0016791	phosphatase activity
MF	GO:0030246	carbohydrate binding
MF	GO:0008289	lipid binding
CC	GO:0031966	mitochondrial membrane
CC	GO:0070013	intracellular organelle lumen
CC	GO:0016324	apical plasma membrane
CC	GO:0005743	mitochondrial inner membrane
CC	GO:0019866	organelle inner membrane
KEGG	mmu01100	Metabolic pathways
KEGG	mmu03050	Other glycan degradation
KEGG	mmu04146	Valine, leucine and isoleucine degradation
KEGG	mmu05017	Propanoate metabolism
KEGG	mmu04961	Glyoxylate and dicarboxylate metabolism

Fig. 8 GO and KEGG enrichment analysis in HFD/NFD mice. GO and KEGG analysis of up-regulated DEPs in the HFD/NFD group (**A**); GO and KEGG analysis of down-regulated DEPs in the HFD/NFD group (**B**). Abbreviations: GO, Gene Ontology; BP, biological processes; CC, cell components; MF, molecular function; KEGG, Kyoto Encyclopedia of Genes and Genomes; NFD, normal-fat diet; HFD, high-fat die

in Vasopressin-regulated water reabsorption, platelet activation, oxidative phosphorylation, regulation of actin cytoskeleton, and PPAR signaling pathway (Fig. 10B).

Screening for ORG-related deps

Quantitative association among kidney DEPs in all groups of mice was illustrated using a Venn diagram, which identified approximately 45 DEPs that were expressed in HFD/NFD, HS/HFD, and HA/HFD mice (Fig. 11A). When these 45 DEPs were imported into the STRING online database, it was found that 39 of them displayed interactions, and the interaction network of these DEPs was visualized using Cytoscape software (Fig. 11B). The Degree algorithm was used to identify the top 10 DEPs with the strongest interactions, which were then analyzed (Fig. 11C). Among the top 10 DEPs, Txn was associated with inflammatory and OS responses. Its expression was elevated in HFD/NFD mice and decreased in HS/HFD and HA/HFD mice (Fig. 11D).

A

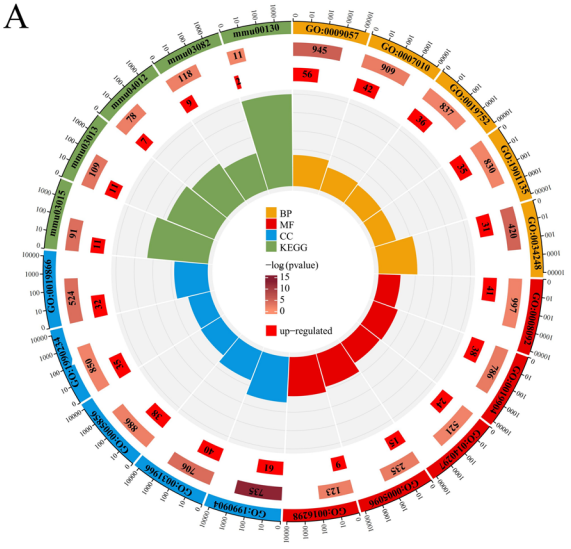

Up-regulated DEPs in HS/HFD

BP	GO:0009057	macromolecule catabolic process
BP	GO:0007010	cytoskeleton organization
BP	GO:0019752	carboxylic acid metabolic process
BP	GO:1901135	carbohydrate derivative metabolic process
BP	GO:0034248	regulation of amide metabolic process
MF	GO:0008092	cytoskeletal protein binding
MF	GO:0019904	protein domain specific binding
MF	GO:0140297	DNA-binding transcription factor binding
MF	GO:0005096	GTPase activator activity
MF	GO:0016298	lipase activity
CC	GO:1990904	ribonucleoprotein complex
CC	GO:0031966	mitochondrial membrane
CC	GO:0005856	cytoskeleton
CC	GO:1990234	transferase complex
CC	GO:0019866	organelle inner membrane
KEGG	mmu03015	mRNA surveillance pathway
KEGG	mmu03013	Nucleocytoplasmic transport
KEGG	mmu04012	ErbB signaling pathway
KEGG	mmu03082	ATP-dependent chromatin remodeling
KEGG	mmu00130	Ubiquinone and other terpenoid-quinone biosynthesis

B

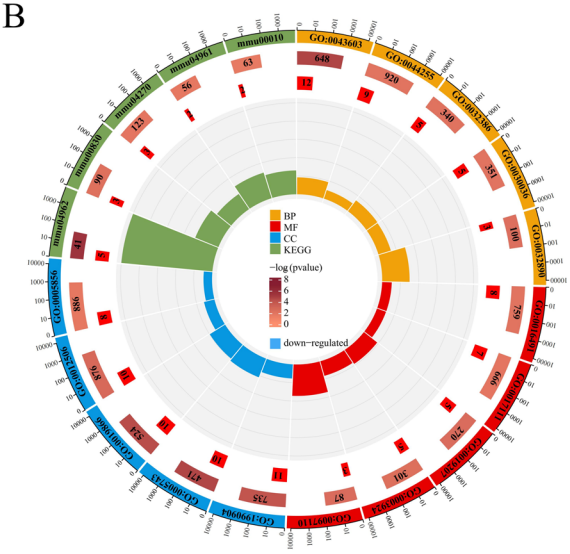

Down-regulated DEPs in HS/HFD

BP	GO:0043603	amide metabolic process
BP	GO:0044255	cellular lipid metabolic process
BP	GO:0032386	regulation of intracellular transport
BP	GO:0030036	actin cytoskeleton organization
BP	GO:0032890	regulation of organic acid transport
MF	GO:0016491	oxidoreductase activity
MF	GO:0017111	ribonucleoside triphosphate phosphatase activity
MF	GO:0019207	kinase regulator activity
MF	GO:0003924	GTPase activity
MF	GO:0097110	scaffold protein binding
CC	GO:1990904	ribonucleoprotein complex
CC	GO:0005743	mitochondrial inner membrane
CC	GO:0019866	organelle inner membrane
CC	GO:0012506	vesicle membrane
CC	GO:0005856	cytoskeleton
KEGG	mmu04962	Vasopressin-regulated water reabsorption
KEGG	mmu00830	Retinol metabolism
KEGG	mmu04270	Vascular smooth muscle contraction
KEGG	mmu04961	Endocrine and other factor-regulated calcium reabsorption
KEGG	mmu00010	Glycolysis / Gluconeogenesis

Fig. 9 GO and KEGG enrichment analysis in HS/HFD mice. GO and KEGG analysis of up-regulated DEPs in the HS/HFD group (**A**); GO and KEGG analysis of down-regulated DEPs in the HS/HFD group (**B**). Abbreviations: GO, Gene Ontology; BP, biological processes; CC, cell components; MF, molecular function; KEGG, Kyoto Encyclopedia of Genes and Genomes; HFD, high-fat die; HS, HFD + semaglutide intervention

KEGG analysis of Txn-related pathways

The Nucleotide-binding Oligomerization Domain (NOD)-like Receptor signaling pathway was identified as the enriched pathway associated with Txn upon its importation into the KEGG online database. Further, Txn was related to the Txnip/NLRP3 signaling pathway in the context of the NOD-like receptor signaling pathway (Fig. 12).

Txnip/NLRP3 signal pathway confirmation via WB

The expression levels of Txn, Txnip, and NLRP3 in HFD mice were significantly higher than those in NFD mice, as demonstrated by Western Blot analysis. Conversely, Txn, Txnip, and NLRP3 expression levels in HS and HA mice were considerably lower than in HFD mice (Fig. 13).

Discussion

ORG has become an important secondary nephropathy that leads to end-stage renal disease (ESRD), which poses a great threat to human health. Normally, ORG patients show proteinuria, and a small number of them may also have kidney failure [13]. Pathological studies have found that ORG mainly manifests as glomerular hypertrophy, glomerular basal membrane thickening, with or without

A

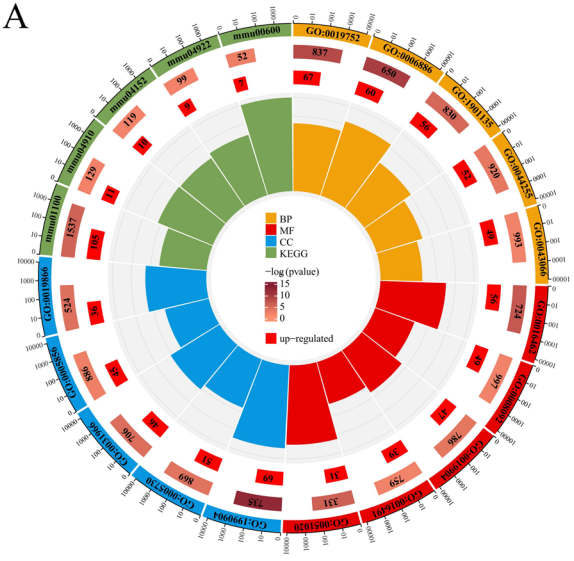

Up-regulated DEPs in HA/HFD

BP	GO:0019752	carboxylic acid metabolic process
BP	GO:0006886	intracellular protein transport
BP	GO:1901135	carbohydrate derivative metabolic process
BP	GO:0044255	cellular lipid metabolic process
BP	GO:0043066	negative regulation of apoptotic process
MF	GO:0016462	pyrophosphatase activity
MF	GO:0008092	cytoskeletal protein binding
MF	GO:0019904	protein domain specific binding
MF	GO:0016491	oxidoreductase activity
MF	GO:0051020	GTPase binding
CC	GO:1990904	ribonucleoprotein complex
CC	GO:0005730	nucleolus
CC	GO:0031966	mitochondrial membrane
CC	GO:0005856	cytoskeleton
CC	GO:0019866	organelle inner membrane
KEGG	mmu01100	Metabolic pathways
KEGG	mmu04910	Insulin signaling pathway
KEGG	mmu04152	AMPK signaling pathway
KEGG	mmu04922	Glucagon signaling pathway
KEGG	mmu00600	Sphingolipid metabolism

B

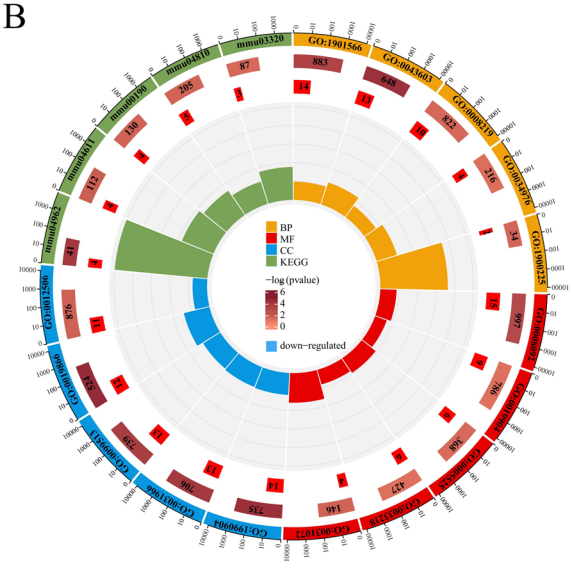

Down-regulated DEPs in HA/HFD

BP	GO:1901566	organonitrogen compound biosynthetic process
BP	GO:0043603	amide metabolic process
BP	GO:0008219	cell death
BP	GO:0034976	response to endoplasmic reticulum stress
BP	GO:1900225	regulation of NLRP3 inflammasome complex assembly
MF	GO:0008092	cytoskeletal protein binding
MF	GO:0019904	protein domain specific binding
MF	GO:0005525	GTP binding
MF	GO:0033218	amide binding
MF	GO:0031072	heat shock protein binding
CC	GO:1990904	ribonucleoprotein complex
CC	GO:0031966	mitochondrial membrane
CC	GO:0099513	polymeric cytoskeletal fiber
CC	GO:0019866	organelle inner membrane
CC	GO:0012506	vesicle membrane
KEGG	mmu04962	Vasopressin-regulated water reabsorption
KEGG	mmu04611	Platelet activation
KEGG	mmu00190	Oxidative phosphorylation
KEGG	mmu04810	Regulation of actin cytoskeleton
KEGG	mmu03320	PPAR signaling pathway

Fig. 10 GO and KEGG enrichment analysis in HA/HFD mice. GO and KEGG analysis of up-regulated DEPs in the HA/HFD group (**A**); GO and KEGG analysis of down-regulated DEPs in the HA/HFD group (**B**). Abbreviations: GO, Gene Ontology; BP, biological processes; CC, cell components; MF, molecular function; KEGG, Kyoto Encyclopedia of Genes and Genomes; HFD, high-fat die; HA, HFD + adenosine intervention

glomerulosclerosis [14]. Under electron microscopy, the reduction in the number of podocyte, podocyte fusion can be observed [15].

Obesity is a persistent low-grade inflammation and chronic OS. Adipocytes possess endocrine functions and release leptin, adiponectin, other adipokines, and inflammatory mediators. In obese individuals, adipose tissue secretes a higher amount of leptin, which enhances the synthesis of type IV collagen mRNA, thus promoting glomerulosclerosis [16]. Adiponectin can regulate the function of renal podocytes and maintain the glomerular filtration barrier. However, the secretion of adiponectin by adipocytes decreases in cases of obesity [17]. Moreover, leptin and adiponectin are intricately associated with inflammatory responses and may regulate TNF-α expression via distinct mechanisms [18]. Besides TNF-α, inflammatory mediators, including IL-6, IL-1β, and monocyte chemoattractant protein-1 (MCP-1), have shown elevated production, worsening insulin resistance and apoptosis, and contributing to renal impairment [19]. Under the excessive immune response of fatty tissue, ROS production increases, and ROS-mediated

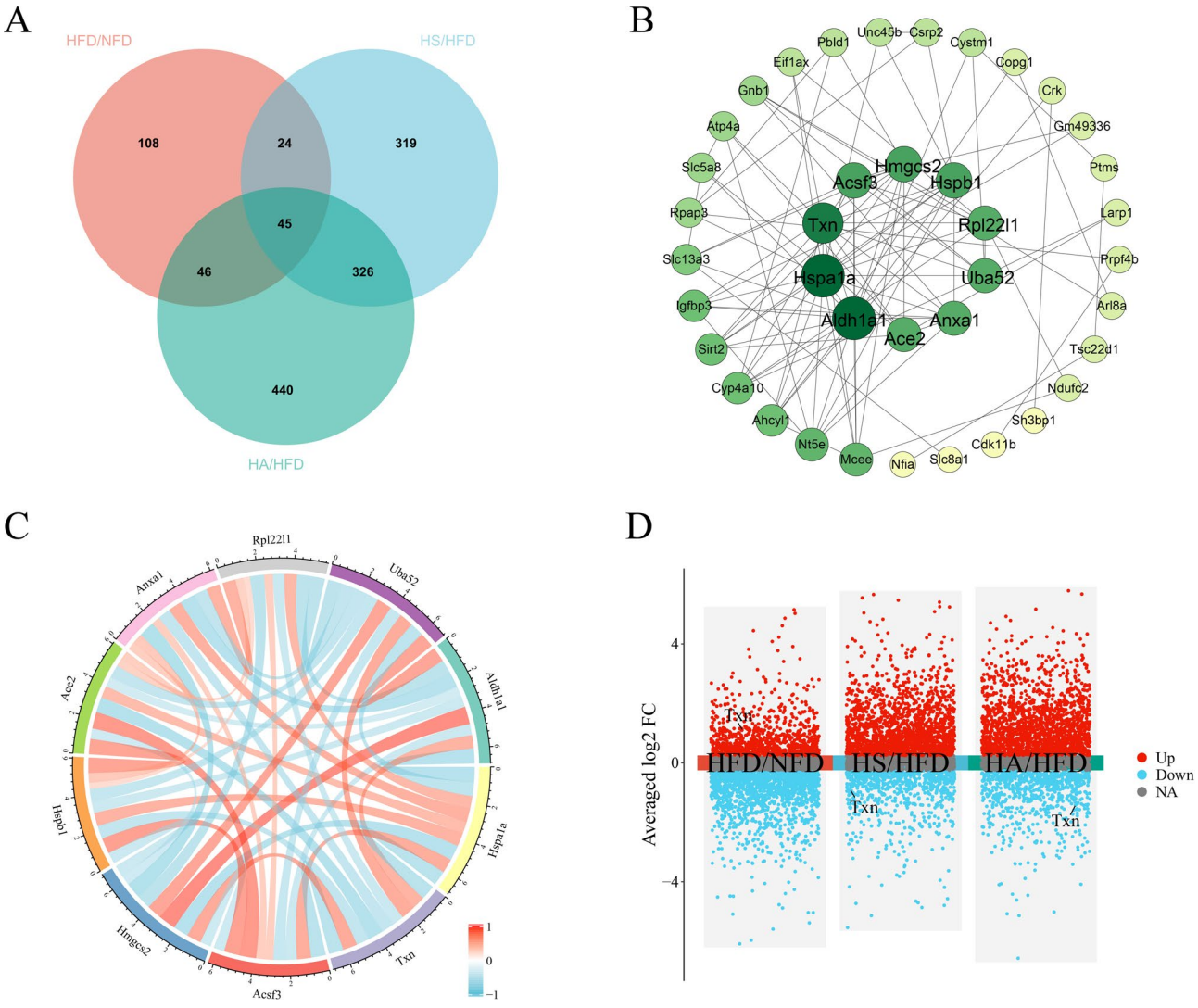

Fig. 11 PPI Network Analysis for DEPs. Venn diagrams analysis of mouse kidney protein (**a**); PPI Network Analysis for DEPs (**B**); Correlation analysis of the top 10 DEPs (**C**); Expression trend of Txn in different groups (**D**)

oxidative damage promotes proximal renal tubular oxidative apoptosis, leading to proteinuria [18]. Simultaneously, OS is frequently used as the upstream phase of the inflammatory cascades, resulting in a malignant cycle characterized by inflammatory reactions. In our study, the UACR of obese mice also increased substantially, and the weight, glucose and lipid metabolism, inflammation, and OS levels of HFD mice were significantly higher than those of NFD mice. In HFD mice, pathology indicated glomerular enlargement, tubular injury, and renal interstitial fibrosis. Simultaneously, the renal basement membrane thickening, podocyte fusion, and glomerular podocyte injury were observed under electron microscopy. The ORG mouse model has been successfully shaped, and this demonstrates that obesity induced by an HFD has a negative effect on the structure and function of the kidneys of mice.

Semaglutide is a GLP-1 analog, an intestinal peptide hormone secreted by L cells, which can improve IR, maintain blood sugar homeostasis, suppress the appetite center, and lose weight [20]. Semaglutide activates the AMPK in the medial nucleus of the hypothalamus to promote the heat production of brown adipose tissue and the browning of white adipose tissue. Activated AMPK liberates free fatty acids and upregulates uncoupling protein-1 (UCP1) via the brown adipocyte cAMP/PKA pathway, promoting lipolysis [21]. In clinical settings, semaglutide can decrease basal weight by 20–30% and shows fewer adverse effects, confirming it is a novel method for managing obesity-related metabolic disorders [22]. Simultaneously, semaglutide can enhance and protect multi-organ health by improving metabolism, bolstering antioxidant defenses, suppressing inflammation, promoting autophagy, strengthening gut microbiota,

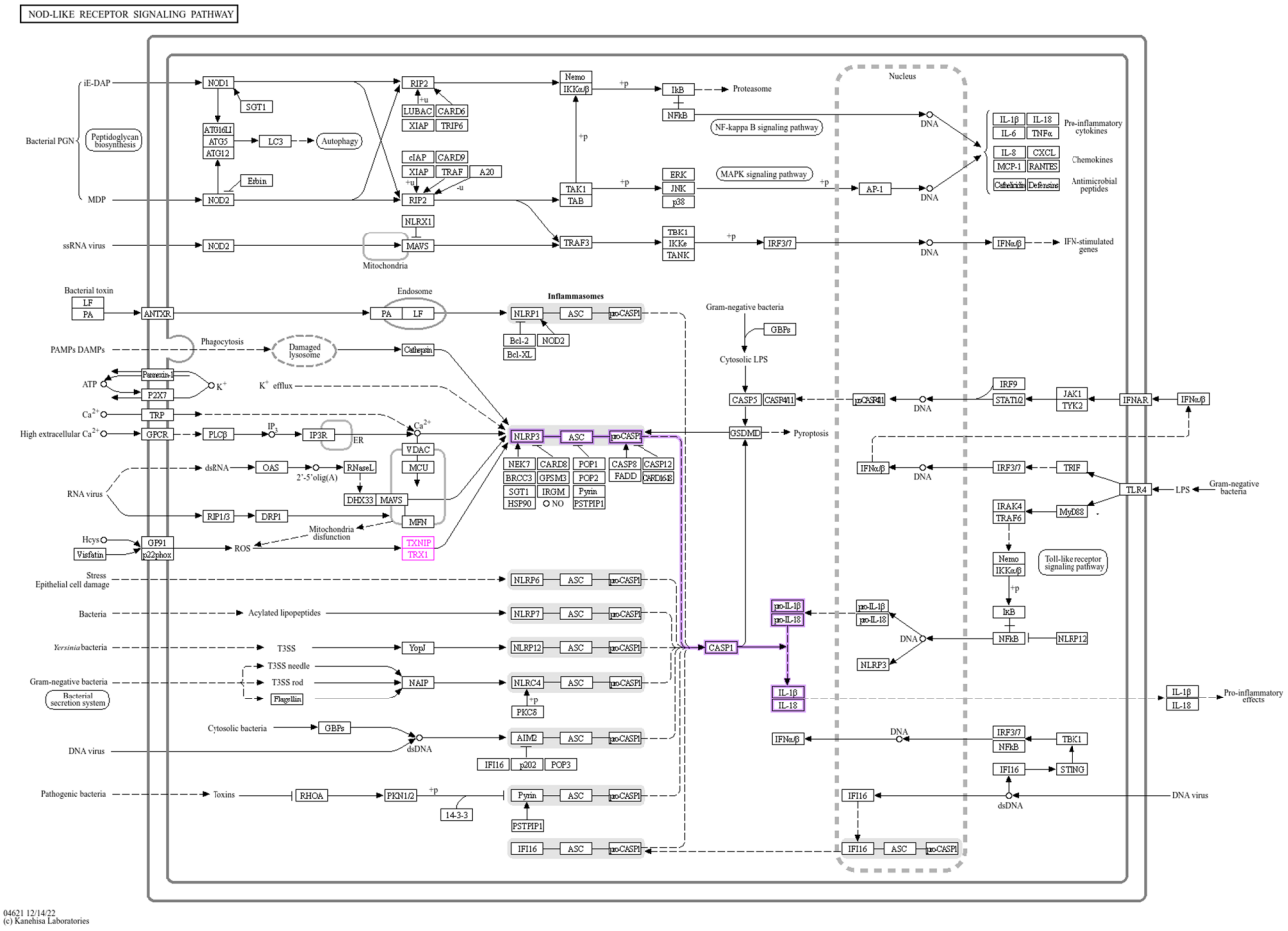

Fig. 12 NOD-like receptor signaling system. Note: The figure is from the KEGG website (https://www.kegg.jp/kegg/mapper/)

and enhancing DNA repair [23]. Adenosine is a purine nucleotide composed of adenine and ribose. The primary sources of adenosine are the dephosphorylation of adenosine triphosphate (ATP) and S-adenosylhomocysteine degradation [24]. In the physiological state, extracellular adenosine levels are maintained at a low concentration. When extracellular adenosine levels increase, adenosine is transported to the intracellular to facilitate ATP synthesis or metabolized into inosine to participate in the purine synthesis pathway [25]. Moreover, adenosine affects various signaling pathways by binding to G protein-coupled adenosine receptors (A1, A2a, A2b, A3), providing physiological functions such as vasoconstriction, anti-inflammatory effects, immune suppression, neuroprotection, antioxidant activity, and anti-apoptotic mechanisms 26]. Recent research indicates that adenosine stimulates brown adipose tissue via the A2a receptor, establishing it as a novel target for anti-obesity treatment [11. Adenosine metabolite inosine stimulates cAMP signaling and energy consumption in brown adipocytes. Inosine injection can enhance the resistance of mice to obesity caused by an HFD [27]. Adenosine widely participates in cellular energy metabolism and signal transduction through four distinct G-protein-coupled receptors. The adenosine signaling pathway is a crucial molecular mechanism regulating various physiological and pathological processes in the body. In recent studies on semaglutide, it was found that differential metabolites in the kidneys of obese mice after semaglutide intervention were significantly enriched in the adenosine signaling pathway. This suggests that semaglutide may exert renal protective effects through the adenosine pathway [9]. We gave semaglutide or adenosine intervention during high-fat dietary feeding. It was found that semaglutide and adenosine can reduce the weight of obese mice, and improve the blood glucose metabolism, blood lipid metabolism, inflammation and OS levels of obese mice to varying degrees. At the same time, lipid deposition in the kidneys of mice was significantly reduced, and glomerular and renal tubular damage were relatively alleviated, indicating the protective effect of semaglutide and adenosine on the kidneys of obese mice.

This study further used proteomics technology to analyze the protective effects of semaglutide and adenosine

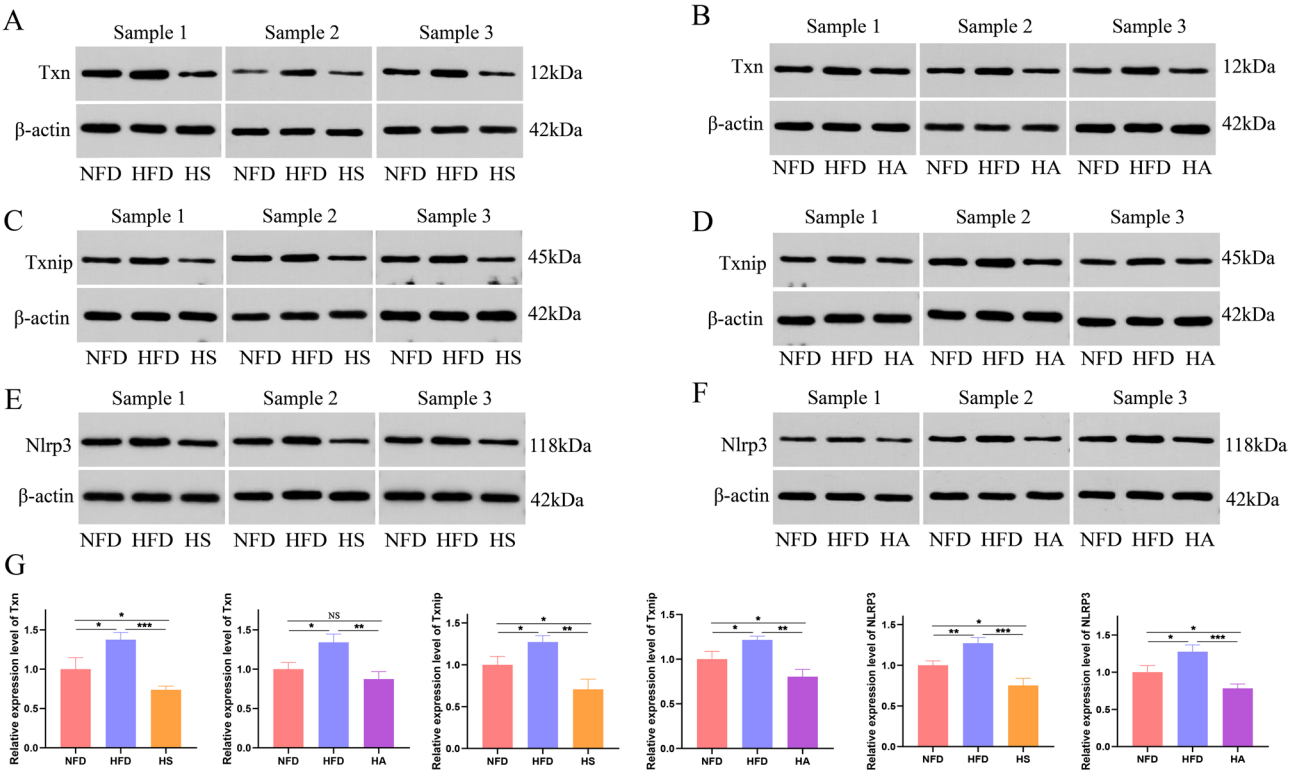

Fig. 13 Western Blot analyses of Txn, Txnip, NLRP3. Expression of Txn in the kidneys of NFD, HFD and HS mice (**A**); Expression of Txn in the kidneys of NFD, HFD and HA mice (**B**); Expression of Txnip in the kidneys of NFD, HFD and HS mice (**C**); Expression of Txnip in the kidneys of NFD, HFD and HA mice (**D**); Expression of Nlrp3 in the kidneys of NFD, HFD and HS mice (**E**); Expression of Nlrp3 in the kidneys of NFD, HFD and HA mice (**F**); Quantitative analysis of Txn, Txnip and NLRP3 in the kidneys, $n = 3$, repeat 3 experiments (**G**). Note: *Denotes significance at a P value of < 0.05, **Denotes significance at a P value of < 0.01, ***Denotes significance at a P value of < 0.001. Abbreviations: NFD, normal-fat diet; HFD, high-fat die; HS, HFD + semaglutide intervention; HA, HFD + adenosine intervention; Txn, Thioredoxin; Txnip, Thioredoxin-Interacting Protein; NLRP3, Nod-Like Receptor Protein 3

on the kidneys. Proteins and signaling pathways related to lipid metabolism, energy metabolism, inflammation and redox reactions have changed significantly in different intervention situations. We used Venn diagrams to identify DEPs that coexist in the HFD/NFD, HS/HFD, and HA/HFD groups. These DEPs were examined by Protein-Protein Interaction Networks (PPI) to detect the 10 most interacting proteins among the DEPs. After analyzing the first 10 proteins, Thioredoxin (Txn) was found to be associated with inflammation and OS. After KEGG analysis of Txn, it was found that Txn was mainly enriched in the Nucleotide-binding oligomerization domain (NOD)-like receptor signaling pathway. NOD-like receptor signaling pathways participate in cellular immune response, which is associated with promoting inflammatory response and inducting cell pyroptosis. Studies indicated that the Yishen capsule, used for diabetic nephropathy, lowered proteinuria in rats and ameliorated renal damage in diabetic rats by inhibiting NOD-like receptor signaling pathways [28]. Txn belongs to the Txnip/NLRP3 pathway, which is a component of the NOD-like receptor signaling system. Trx1 is encoded and synthesized by the Txn gene. Trx1 interacts with Thioredoxin-Interacting Protein (Txnip) and remains stable under physiological conditions. In the event of OS, the Trx1/Txnip complex dissociation is induced by an increase in ROS formation. After Trx1/Txnip complex dissociation, Txnip and Nod-Like Receptor Protein 3 (NLRP3) interact to produce apoptotic protein caspase-1 and pro-inflammatory factors IL-1β and IL-18 [29]. ROS/Txnip/NLRP3 signaling pathways have been widely confirmed in disease models of neurodegenerative lesions and non-alcoholic fatty liver, which promotes inflammatory response and apoptosis by inducing NLRP3 inflammasome activation [30, 31, 32]. NLRP3 inflammasome is an intracellular polyprotein complex (NLRP3/ASC/caspase-1 complex), including NLRP3, apoptosis-related spot-like protein (ASC), and caspase-1. Txnip-mediated NF-κB signaling pathway and intracellular Txnip transfer are one of the ways to activate NLRP3 inflammasome [33]. Currently, the activation and regulation of NLRP3 inflammasomes in chronic inflammatory responses remains a focal point of investigation. Over-activation of NLRP3 inflammasome is related to non-alcoholic fatty liver, renal fibrosis, inflammatory bowel disease, neurodegenerative lesions, atherosclerosis, and other diseases [34, 35, 36, 37,

38]. During the activation of NLRP3, various pathogen-associated molecular patterns (PAMPs) and damage-associated molecular patterns (DAMPs) promote NLRP3 inflammasome assembly through different molecular and cellular events, such as K + excretion, Cl – excretion, Ca2 + signal conduction, mitochondrial dysfunction, ROS release, lysosome destruction, and promote IL-1β and IL-18 maturity [39]. Similarly, the activation of caspase-1 cleaves Gasdermin D (GSDMD), resulting in membrane pore formation and pyroptosis [40]. NLRP3 inflammasome plays a significant role in chronic kidney injury. In patients with lupus nephritis, the increase in urine protein levels is associated with the accumulation of NLRP3 in the glomerus [41]. The level of NLRP3 mRNA in peripheral blood mononuclear cells of patients with chronic Kidney disease (CKD) on long-term hemodialysis is significantly higher than that of healthy people [42]. In mice with diabetic nephropathy, inhibition of NLRP3, ASC or caspase-1 can reduce the damage of tubular stromal cells, endothelial cells and membrane cells, as well as the inflammatory response of tubular interstitial cells [43]. After the knockdown of NLRP3 in diabetic mice, NF-κB/p65 activation and mitochondrial ROS production decreased, sterol regulatory element-binding protein 1 (SREBP1)-mediated podocyte lipid metabolism signaling pathway was inhibited, and diabetes-induced loss of renal podocyte and glomerular fat accumulation was reversed [44]. In the mice model of diabetic nephropathy, it was found that endoplasmic reticulum stress can also activate the Txnip/NLRP3 pathway. When the expression of endoplasmic reticulum stress-related factors (ATF4, CHOP, and IRE1α) was elevated, the upregulation of IRE1α enhanced the degradation of miR-200a, activated the Txnip/NLRP3 pathway, and promoted pyroptosis and renal injury [45]. Therefore, kidney injury necessitates consideration of the Txnip/NLRP3 signaling pathway and NLRP3 inflammasome.

Previous studies have shown that GLP-1 receptor agonist can inhibit the excessive accumulation of ROS by enhancing mitochondrial autophagy, thus inhibiting NLRP3 inflammasome-induced pyroptosis and play a protective role in the heart and liver [46–47]. The injection of Liraglutide or Semaglutide during the propagation of renal podocytes under hyperglycemic conditions can suppress the expression of NF-κB p65, NLRP3, GSDMD, caspase-1, IL-1β, and IL-18 [48]. Extracellular adenosine triphosphate (ATP) is frequently considered an inflammatory agent, as it stimulates the activation of P2 purine receptors and NLRP3 inflammasomes. However, at the same time, extracellular ATP can be converted into adenosine through CD39 and CD73 on the cell surface, playing an anti-inflammatory role through the P1 purine receptor to regulate extracellular ATP and adenosine and regulate the immune inflammatory response [49]. Extracellular adenosine interacts with adenosine A2b receptors in hematopoietic stem cells, increasing intracellular cAMP and Nrf2 levels, stimulation of the antioxidant stress pathway, and a variation of the level of heme oxygenase-1 (HO-1). HO-1 reduces the expression of NLRP3, ASC, and caspase-1, hinders the stimulation of the NLRP3 inflammasomes, and regulates the formation of hematopoietic stem cells and progenitor cells [50]. GLP-1 agonists and adenosine can inhibit inflammatory reactions by inhibiting the activation of NLRP3 inflammasomes, thus playing a multi-organ protective role. In our experiment, Txn, Txnip, and NLRP3 in the kidneys of HFD mice were significantly higher than those of NFD mice. After the intervention of semaglutide and adenosine, the expression of Txn, Txnip, and NLRP3 decreased. The study also verified IL-18, the end product of the Txnip/NLRP3 signaling pathway, and found that the level of IL-18 in the kidneys of HFD mice was significantly higher than that of NFD mice and decreased after intervention with semaglutide and adenosine. This study used a proteomics approach to identify the kidney-critical proteins Txn and Txnip/NLRP3 signaling pathways. Next, WB and ELISA were performed to confirm the protein and end products of the pathway. The activation of NLRP3 inflammatory bodies can be inhibited by semaglutide and adenosine, which may serve as a novel treatment strategy for ORG by reducing the Txnip/NLRP3 signaling pathway in the kidney. However, although semaglutide has significant renal protective effects, some literature reports suggest that its use may lead to acute kidney injury through mechanisms such as vomiting and diarrhea, which alter renal blood flow [51]. In these cases, the deterioration of renal function in patients is directly temporally associated with the use of semaglutide [51]. Therefore, for patients with pre-existing kidney issues, both doctors and patients need to be more vigilant about the potential renal risks associated with this medication.

The study has some limitations. First, our WB results were derived from three biological replicates, with missing technical replicates, which was an oversight in our experimental design. The WB results should be interpreted with caution. And the results may be associated with the current experimental subjects and the duration and dosage of the drug intervention.The described molecular mechanism needs to be further verified at the cellular and clinical levels, which is also the focus of our next stage. Additionally, the absence of female mice in our study limits the generalizability of our experimental results. Further investigation is required to explore the potential therapeutic applications of semaglutide and adenosine in female patients with obesity-related kidney disease.

Conclusion

The conclusion of this study was that semaglutide and adenosine significantly decrease the weight of obese mice and actively improve the damage to kidney structure and function caused by obesity. Moreover, significant alterations in the TXNIP/NLRP3 signaling pathway were observed across intervention groups, suggesting its potential role as a molecular mechanism underlying the renoprotective effects of these drugs.

Acknowledgements
Not applicable.

Author contributions
SC.C. designed and supervised the study. SQ.W. and XY.P. completed the experiment and analyzed the data. SQ.W. and RQ.L. wrote the manuscript, XY.P. drew figures. All authors have read and approved the final manuscript.

Funding
This study was supported by the Hebei Province Natural Science Foundation (H2022307026).

Data availability
The original data presented in the study are included in the article/Supplementary Material. Further inquiries can be directed to the corresponding author.

Declarations

Ethics approval and consent to participate
All experiments and procedures were conducted in accordance with the Regulations on the Management of Laboratory Animals issued by the National Science and Technology Commission and were approved by the Animal Ethics Association of the Hebei General Hospital (Approval Number:202332). The ARRIVE criteria were adopted in all animal trials.

Consent for publication
Not applicable.

Competing interests
The authors declare no competing interests.

Received: 29 January 2025 / Accepted: 11 May 2025
Published online: 24 May 2025

References

1. Stasi A, Cosola C, Caggiano G, et al. Obesity-Related chronic kidney disease: principal mechanisms and new approaches in nutritional management. Front Nutr. 2022. https://doi.org/10.3389/fnut.2022.925619. 9 Front Nutr.
2. Lobstein T, Jackson-Leach R, Brinsden H, Gray M. World obesity atlas 2023. London, UK: World Obesity Federation; 2023.
3. Ansari S, Haboubi H, Haboubi N. Adult obesity complications: challenges and clinical impact. Ther Adv Endocrinol Metab. 2020;11:2042018820934955. https://doi.org/10.1177/2042018820934955. PMID: 32612803; PMCID: PMC7309384.
4. Zhao S, Xu X, You H, Ge J, Wu Q. Healthcare costs attributable to abnormal weight in China: evidence based on a longitudinal study. BMC Public Health. 2023;23(1):1927. https://doi.org/10.1186/s12889-023-16855-6. PMID: 37798694; PMCID: PMC10552200.
5. Kambham N, Markowitz GS, Valeri AM, Lin J, D'Agati VD. Obesity-related glomerulopathy: an emerging epidemic. Kidney Int. 2001;59(4):1498– 509. https://doi.org/10.1046/j.1523-1755.2001.0590041498.x. PMID: 11260414.
6. Garofalo C, Borrelli S, Minutolo R, Chiodini P, De Nicola L, Conte G. A systematic review and meta-analysis suggests obesity predicts onset of chronic kidney disease in the general population. Kidney Int. 2017;91(5):1224–35. Epub 2017 Feb 7. PMID: 28187985.
7. Sandino J, Martín-Taboada M, Medina-Gómez G, Vila-Bedmar R, Morales E. Novel insights in the physiopathology and management of Obesity-Related kidney disease. Nutrients. 2022;14(19):3937. https://doi.org/10.3390/nu14193937. PMID: 36235590; PMCID: PMC9572176.
8. Liu Y, Luo X. New practice in semaglutide on type-2 diabetes and obesity: clinical evidence and expectation. FRONT MED-PRC. 2022. https://doi.org/10.1007/s11684-021-0873-2. 16 FRONT MED-PRC.
9. Chen X, Chen S, Ren Q, et al. Metabolomics provides insights into renoprotective effects of semaglutide in obese mice. Drug Des Devel Ther. 2022;16. https://doi.org/10.2147/DDDT.S383537. Drug Des Devel Ther.
10. Pasquini S, Contri C, Borea PA, Vincenzi F, Varani K. Adenosine and inflammation: here, there and everywhere. Int J Mol Sci. 2021;22(14):7685. https://doi.org/10.3390/ijms22147685. PMID: 34299305; PMCID: PMC8304851.
11. Gnad T, Scheibler S, von Kügelgen I, et al. Adenosine activates brown adipose tissue and recruits beige adipocytes via A2A receptors. Nature. 2014;516(7531):395–9. https://doi.org/10.1038/nature13816. Epub 2014 Oct 15. PMID: 25317558.
12. Kaster MP, Rosa AO, Rosso MM et al. Adenosine administration produces an antidepressant-like effect in mice: evidence for the involvement of A1 and A2A receptors. NEUROSCI LETT. 2004; 355 NEUROSCI LETT. https://doi.org/10.1016/j.neulet.2003.10.040
13. Herman-Edelstein M, Weinstein T, Chagnac A, Obesity-Related, Glomerulopathy. Clinical Management. SEMIN NEPHROL. 2021; 41 SEMIN NEPHROL. https://doi.org/10.1016/j.semnephrol.2021.06.007
14. Yang S, Cao C, Deng T, et al. Obesity-Related glomerulopathy: A latent change in obesity requiring more attention. KIDNEY BLOOD PRESS R. 2020. https://doi.org/10.1159/000507784. 45 KIDNEY BLOOD PRESS R.
15. Camici M, Galetta F, Abraham N, et al. Obesity-related glomerulopathy and podocyte injury: a mini review. Front Biosci (Elite Ed). 2012. https://doi.org/10.2741/E441. 4 Front Biosci (Elite Ed).
16. Wolf G, Hamann A, Han DC et al. Leptin stimulates proliferation and TGF-beta expression in renal glomerular endothelial cells: potential role in glomerulosclerosis [seecomments]. KIDNEY INT. 1999; 56 KIDNEY INT. https://doi.org/10.1046/j.1523-1755.1999.00626.x
17. Kawarazaki W, Nagase M, Yoshida S, et al. Angiotensin II- and salt-induced kidney injury through Rac1-mediated mineralocorticoid receptor activation. J AM SOC NEPHROL. 2012. https://doi.org/10.1681/ASN.2011070734. 23 J AM SOC NEPHROL.
18. Tang J, Yan H, Zhuang S. Inflammation and oxidative stress in obesity-related glomerulopathy. Int J Nephrol. 2012;2012:608397. https://doi.org/10.1155/2012/608397.
19. Xu H. Obesity and metabolic inflammation. Drug Discov Today Dis Mech. 2013; 10 Drug Discov Today Dis Mech. PMID: 24003334.
20. Yang XD, Yang YY. Clinical pharmacokinetics of semaglutide: A systematic review. Drug Des Devel Ther. 2024. https://doi.org/10.2147/DDDT.S470826. 18 Drug Des Devel Ther.
21. Tamayo-Trujillo R, Ruiz-Pozo VA, Cadena-Ullauri S et al. Molecular mechanisms of semaglutide and liraglutide as a therapeutic option for obesity. Front Nutr. 2024; 11 Front Nutr. https://doi.org/10.3389/fnut.2024.1398059
22. Aroda VR, Ahmann A, Cariou B et al. Comparative efficacy, safety, and cardiovascular outcomes with once-weekly subcutaneous semaglutide in the treatment of type 2 diabetes: Insights from the SUSTAIN 1–7 trials. DIABETES METAB. 2019; 45 DIABETES METAB. https://doi.org/10.1016/j.diabet.2018.12.001
23. Bradley CL, McMillin SM, Hwang AY, et al. High-Dose Once-Weekly semaglutide: A new option for obesity management. ANN PHARMACOTHER. 2022. https://doi.org/10.1177/10600280211053867. 56 ANN PHARMACOTHER.
24. Ham J, Evans BA. An emerging role for adenosine and its receptors in bone homeostasis. Front Endocrinol (Lausanne). 2012. https://doi.org/10.3389/fendo.2012.00113. 3 Front Endocrinol (Lausanne).
25. Cristalli, G, Costanzi, S, Lambertucci, C, et al. Adenosine deaminase: functional implications and different classes of inhibitors. MED RES REV. 2001; 21 MED RES REV. doi: 10.1002/1098-1128(200103)21:2<105::aid-med1002>3.0.co;2-u.
26. Sachdeva S, Gupta M. Adenosine and its receptors as therapeutic targets: an overview. SAUDI PHARM J. 2013;21(SAUDI PHARM J). https://doi.org/10.1016/j.jsps.2012.05.011.
27. Niemann B, Haufs-Brusberg S, Puetz L et al. Apoptotic brown adipocytes enhance energy expenditure via extracellular inosine. NATURE. 2022; 609 NATURE. https://doi.org/10.1038/s41586-022-05041-0
28. Zhang Z, Hu Y, Liu W, et al. Yishen capsule alleviated symptoms of diabetic nephropathy via NOD-like receptor signaling pathway. Diabetes Metab Syndr

Obes. 2022. https://doi.org/10.2147/DMSO.S368867. 15 Diabetes Metab Syndr Obes.
29. Chu FX, Wang X, Li B et al. The NLRP3 inflammasome: a vital player in inflammation and mediating the anti-inflammatory effect of CBD. INFLAMM RES. 2024; 73 INFLAMM RES. https://doi.org/10.1007/s00011-023-01831-y
30. Zhao Q, Liu G, Ding Q et al. The ROS/TXNIP/NLRP3 pathway mediates LPS-induced microglial inflammatory response. CYTOKINE. 2024; 181 CYTOKINE. https://doi.org/10.1016/j.cyto.2024.156677
31. Zhang M, Ding ZX, Huang W et al. Chrysophanol exerts a protective effect against Aβ25-35-induced Alzheimer's disease model through regulating the ROS/TXNIP/NLRP3 pathway. INFLAMMOPHARMACOLOGY. 2023; 31 INFLAMMOPHARMACOLOGY. https://doi.org/10.1007/s10787-023-01201-4
32. Jiang X, Li Y, Fu D et al. Caveolin-1 ameliorates acetaminophen-aggravated inflammatory damage and lipid deposition in non-alcoholic fatty liver disease via the ROS/TXNIP/NLRP3 pathway. INT IMMUNOPHARMACOL. 2023; 114 INT IMMUNOPHARMACOL. https://doi.org/10.1016/j.intimp.2022.109558
33. Kim SK, Choe JY, Park KY. TXNIP-mediated nuclear factor-κB signaling pathway and intracellular shifting of TXNIP in uric acid-induced NLRP3 inflammasome. BIOCHEM BIOPH RES CO. 2019; 511 BIOCHEM BIOPH RES CO. https://doi.org/10.1016/j.bbrc.2019.02.141
34. Wu C, Bian Y, Lu B et al. Rhubarb free anthraquinones improved mice nonalcoholic fatty liver disease by inhibiting NLRP3 inflammasome. J Transl Med. 2022; 20 J Transl Med. https://doi.org/10.1186/s12967-022-03495-4
35. Li S, Lin Q, Shao X et al. NLRP3 inflammasome inhibition attenuates cisplatin-induced renal fibrosis by decreasing oxidative stress and inflammation. EXP CELL RES. 2019; 383 EXP CELL RES. https://doi.org/10.1016/j.yexcr.2019.07.001
36. Perera AP, Kunde D, Eri R. NLRP3 inhibitors as potential therapeutic agents for treatment of inflammatory bowel disease. CURR PHARM Des. 2017. https://doi.org/10.2174/1381612823666170201162414. 23 CURR PHARM DESIGN.
37. Qiao C, Dang T, Zhou Y et al. Targeting microglial NLRP3 in the SNc region as a promising disease-modifying therapy for Parkinson's disease. Brain Behav. 2022; 12 Brain Behav. https://doi.org/10.1002/brb3.2784
38. Shi X, Xie WL, Kong WW, et al. Expression of the NLRP3 inflammasome in carotid atherosclerosis. J STROKE CEREBROVASC. 2015. https://doi.org/10.1016/j.jstrokecerebrovasdis.2015.03.024. 24 J STROKE CEREBROVASC.
39. Wei L, Li Y, Yu Y, et al. Obesity-Related glomerulopathy: from mechanism to therapeutic target. Diabetes Metab Syndr Obes. 2021;14. https://doi.org/10.2147/DMSO.S334199. Diabetes Metab Syndr Obes.
40. Miao R, Jiang C, Chang WY et al. Gasdermin D permeabilization of mitochondrial inner and outer membranes accelerates and enhances pyroptosis. IMMUNITY. 2023; 56 IMMUNITY. https://doi.org/10.1016/j.immuni.2023.10.004
41. Huang G, Zhang Y, Zhang Y, et al. Chronic kidney disease and NLRP3 inflammasome: pathogenesis, development and targeted therapeutic strategies. Biochem Biophys Rep. 2023. https://doi.org/10.1016/j.bbrep.2022.101417. 33 Biochem Biophys Rep.
42. Zhang K, Fan C, Cai D et al. Contribution of TGF-Beta-Mediated NLRP3-HMGB1 Activation to Tubulointerstitial Fibrosis in Rat With Angiotensin II-Induced Chronic Kidney Disease. Front Cell Dev Biol. 2020; 8 Front Cell Dev Biol. https://doi.org/10.3389/fcell.2020.00001
43. Wang Y, Sui Z, Wang M et al. Natural products in attenuating renal inflammation via inhibiting the NLRP3 inflammasome in diabetic kidney disease. Front Immunol. 2023; 14 Front Immunol. https://doi.org/10.3389/fimmu.2023.1196016
44. Wu M, Yang Z, Zhang C, et al. Inhibition of NLRP3 inflammasome ameliorates podocyte damage by suppressing lipid accumulation in diabetic nephropathy. METABOLISM. 2021;118(METABOLISM). https://doi.org/10.1016/j.metabol.2021.154748.
45. Ke R, Wang Y, Hong S et al. Endoplasmic reticulum stress related factor IRE1α regulates TXNIP/NLRP3-mediated pyroptosis in diabetic nephropathy. EXP CELL RES. 2020; 396 EXP CELL RES. https://doi.org/10.1016/j.yexcr.2020.112293
46. He W, Wei J, Liu X et al. Semaglutide ameliorates pressure overload-induced cardiac hypertrophy by improving cardiac mitophagy to suppress the activation of NLRP3 inflammasome. Sci Rep 2024; 14 Sci Rep. https://doi.org/10.1038/s41598-024-62465-6
47. Yu X, Hao M, Liu Y, et al. Liraglutide ameliorates non-alcoholic steatohepatitis by inhibiting NLRP3 inflammasome and pyroptosis activation via mitophagy. EUR J PHARMACOL. 2019. https://doi.org/10.1016/j.ejphar.2019.172715. 864 EUR J PHARMACOL.
48. Li X, Jiang X, Jiang M et al. GLP-1RAs inhibit the activation of the NLRP3 inflammasome signaling pathway to regulate mouse renal podocyte pyroptosis. ACTA DIABETOL. 2024; 61 ACTA DIABETOL. https://doi.org/10.1007/s00592-023-02184-y
49. Wang C, Yin Q, Su Z et al. [Progress on role of extracellular ATP and its metabolite adenosine in immunoregulation: Review]. Xi Bao Yu Fen Zi Mian Yi Xue Za Zhi. 2020; 36 Xi Bao Yu Fen Zi Mian Yi Xue Za Zhi. PMID: 33325366.
50. Thapa A, Abdelbaset-Ismail A, Chumak V et al. Extracellular Adenosine (eAdo) - A2B Receptor Axis Inhibits in Nlrp3 Inflammasome-dependent Manner Trafficking of Hematopoietic Stem/progenitor Cells. STEM CELL REV REP. 2022; 18 STEM CELL REV REP. https://doi.org/10.1007/s12015-022-10417-w
51. Filippatos TD, Panagiotopoulou TV, Elisaf MS. Adverse Effects of GLP-1 Receptor Agonists. Rev Diabet Stud. 2014. https://doi.org/10.1900/RDS.2014.11.202. 11 Rev Diabet Stud.

Publisher's note